### nature microbiology

**Article** 

https://doi.org/10.1038/s41564-023-01443-6

# Unconventional secretion of *Magnaporthe* oryzae effectors in rice cells is regulated by tRNA modification and codon usage control

Received: 24 May 2022

Gang Li¹, Nawaraj Dulal¹, Ziwen Gong¹² & Richard A. Wilson ©¹⊠

Accepted: 4 July 2023

Published online: 10 August 2023

Check for updates

Microbial pathogens deploy effector proteins to manipulate host cell innate immunity, often using poorly understood unconventional secretion routes. Transfer RNA (tRNA) anticodon modifications are universal, but few biological functions are known. Here, in the rice blast fungus Magnaporthe oryzae, we show how unconventional effector secretion depends on tRNA modification and codon usage. We characterized the *M. oryzae* Uba4-Urm1 sulfur relay system mediating tRNA anticodon wobble uridine 2-thiolation  $(s^2U_{34})$ , a conserved modification required for efficient decoding of AA-ending cognate codons. Loss of s<sup>2</sup>U<sub>34</sub> abolished the translation of AA-ending codon-rich messenger RNAs encoding unconventionally secreted cytoplasmic effectors, but mRNAs encoding endoplasmic reticulum-Golgi-secreted apoplastic effectors were unaffected. Increasing near-cognate tRNA acceptance, or synonymous AA- to AG-ending codon changes in *PWL2*, remediated cytoplasmic effector production in  $\Delta uba4$ . In *UBA4*<sup>+</sup>, expressing recoded *PWL2* caused Pwl2 super-secretion that destabilized the host-fungus interface. Thus, U<sub>34</sub> thiolation and codon usage tune pathogen unconventional effector secretion in host rice cells.

Transfer RNA nucleoside modifications are abundant and occur across all domains of life<sup>1-5</sup>, but biological relevance for many is poorly understood<sup>3,4,6-9</sup>. The genome of the devastating rice blast fungus Magnaporthe oryzae<sup>10-14</sup> carries a UBA4 orthologue (MGG 05569), encoding the evolutionary conserved E1-like Urm1-activating enzyme, and MGG\_03978, encoding the Uba4 substrate ubiquitin related modifier 1 (Urm1). In eukaryotes, Uba4 and Urm1 act together to modify the tRNA wobble uridine-34 anticodon base with sulfur to tune messenger RNA translation<sup>15</sup> (Fig. 1a). tRNA thiolation is a universal modification, but it is not required for general translation and is dispensable in yeast<sup>4</sup>, although its loss affects proteome integrity, metabolic homeostasis and stress responses<sup>3,7,9</sup>. We seek to understand M. oryzae metabolism and growth during rice infection and hypothesized that the M. oryzae Uba4-Urm1 sulfur relay system contributed to fungal colonization of the host rice cell.

The Uba4–Urm1 sulfur relay system is required for 2-thiolation of position 34 wobble uridines ( $s^2U_{34}$ ) in the anticodon loop of cytoplasmic (but not mitochondrial) tRNAs  $^{6,15,16}$  (Fig. 1a).  $s^2U_{34}$  is a universally conserved modification on tRNAs decoding AA-ending cognate codons (i.e., codons carrying adenine in the second and wobble third positions) $^{1-3,7,17}$  (Fig. 1b). A methoxycarbonylmethyl group (mcm) $^5$  also decorates  $U_{34}$ , and the loss of both modifications is lethal $^1$ .  $U_{34}$  thiolation involves the transfer of sulfur from the ubiquitin-like Urm1 following its activation by Uba4 $^{7,15,16,18}$  (Fig. 1a). The loss of  $U_{34}$  thiolation $^7$  slows cognate codon decoding at AA-ending codons, causing ribosome pausing and resulting in reduced translation speeds and increased protein aggregation $^{3,6-8,17}$ . Despite its ubiquity, however, translation defects in  $s^2U_{34}$  mutants are minor $^{3,9}$ , and few physiological roles for the tRNA anticodon wobble  $U_{34}$  thiolation modification are known $^{4,6,7,9,17}$ .

To test our hypothesis that the Uba4–Urm1-mediated 2-thiolation modification of wobble uridines in *M. oryzae* tRNA anticodons

<sup>1</sup>Department of Plant Pathology, University of Nebraska-Lincoln, Lincoln, NE, USA. <sup>2</sup>Present address: State Key Laboratory for Biology of Plant Diseases and Insect Pests, Institute of Plant Protection, Chinese Academy of Agricultural Sciences, Beijing, China. —e-mail: rwilson10@unl.edu

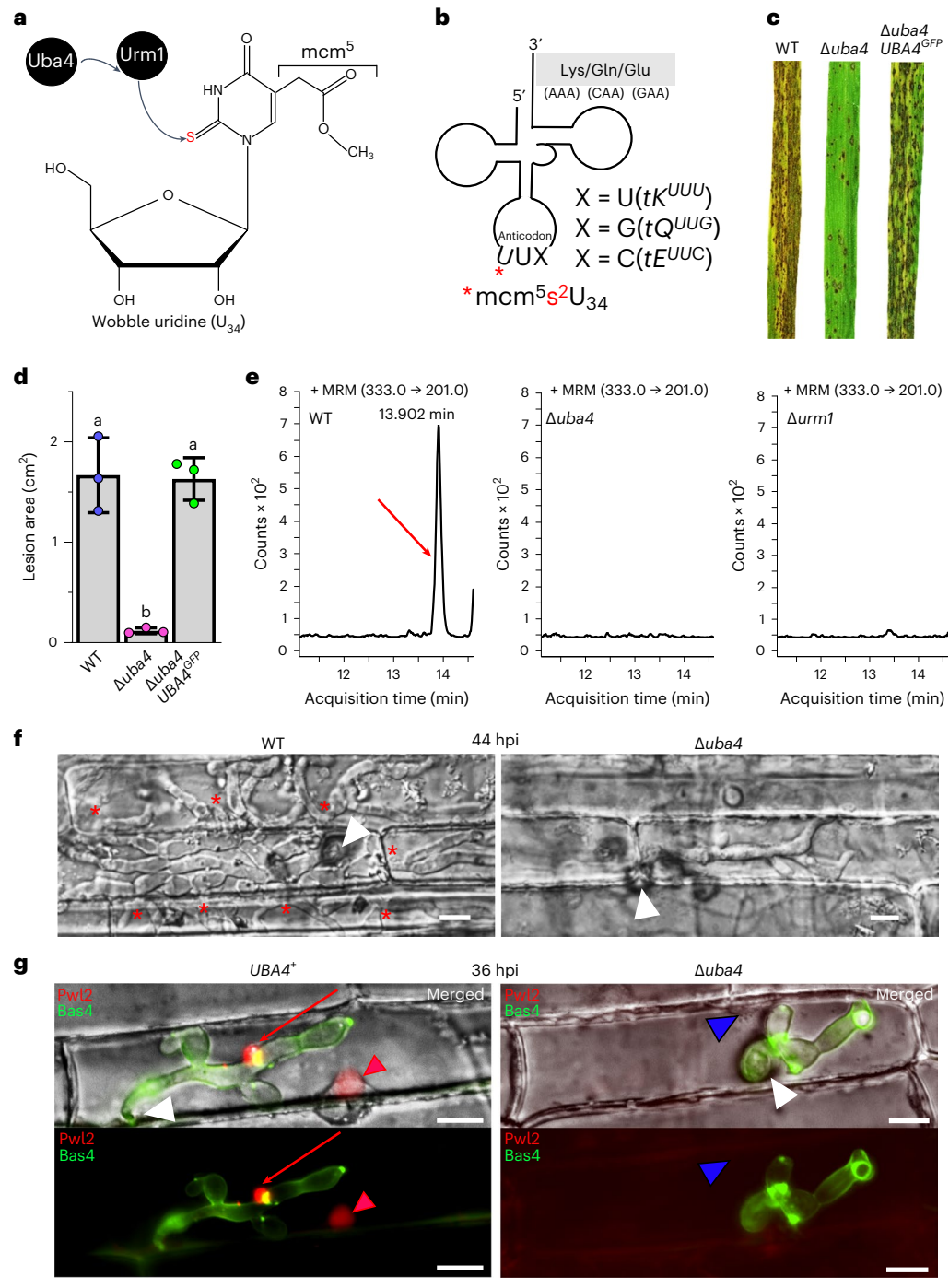


Fig. 1 | tRNA anticodon wobble uridine 2-thiolation is required for fungal pathogenicity. a,b, 2-Thiolation of tRNA anticodon wobble U<sub>34</sub> is mediated by the conserved Uba4–Urm1 sulfur relay system<sup>7</sup> (a) and is a universal modification at tRNA anticodons corresponding to AA-ending codons (b). c, The M. oryzae UBA4 gene is required for pathogenicity on leaves of the susceptible rice cultivar CO-39. Spores of the indicated strains were sprayed on 3-week-old seedlings at a rate of 1 × 105 spores per ml. Images were taken at 5 dpi and are representative of at least 5 leaves from each of 3 independent biological replicates. d, Quantification of rice leaf lesions after 5 dpi following infection with the indicated strains. Disease lesion areas were determined from 10 cm leaf sections using Image J and analysed according to one-way ANOVA followed by Tukey's HSD test for multiple comparison (P < 0.05). Values are means  $\pm$  s.d. calculated from three biological replicates. Different letters above bars indicate significant differences. P = 0.0006 between WT and  $\Delta uba4$ , P = 0.9808 between WT and  $\Delta uba4 UBA4^{GFP}$ , P = 0.0007 between  $\Delta uba4$  and  $\Delta uba4 UBA4^{GFP}$ . **e**, Mass chromatograms of the mcm5s2U tRNA modification in vegetative mycelia of

the indicated strains. The y axes are ion counts; the x axes are acquisition times. The mcm $^5$ s $^2$ U modification peak position is indicated by a red arrow. **f**, Livecell imaging at 44 hpi of detached rice leaf sheath epidermal cells colonized with the indicated strains. White arrowheads indicate penetration sites; red asterisks indicate where IH have spread into neighbouring cells. Scale bars,  $10~\mu m$ . **g**, Live-cell imaging at 36 hpi of detached rice leaf sheath epidermal cells colonized with the indicated strains carrying genes encoding the fluorescent cytoplasmic effector Pwl2-mCherry:NLS and the fluorescent apoplastic effector Bas4-GFP. At this time point, 100% of WT BICs carry Pwl2-mCherry:NLS, but Pwl2-mCherry:NLS fluorescence was not observed in any  $\Delta uba4$ -infected cells. Calculations and representative images are based on the observations of 50 infected rice cells per leaf sheath per treatment; n=3 biological replicates. White arrowheads indicate penetration sites; red arrows indicate Pwl2 in BICs; red arrowheads indicate Pwl2 in host nuclei; blue arrowheads indicate host nuclei without Pwl2. Scale bars,  $10~\mu m$ .

contributes to host plant infection, we functionally characterized the *M. oryzae* Uba4–Urm1 sulfur relay system. In doing so, we discovered a previously unknown connection between tRNA wobble U<sub>34</sub> thiolation-dependent decoding of AA-ending cognate codons, codon usage frequency and the unconventional secretion of *M. oryzae* cytoplasmic effector proteins required for virulence.

#### Results

#### Rice infection and U<sub>34</sub> thiolation requires UBA4 and URM1

To determine whether M. oryzae tRNA thiolation was required for rice infection, we first disrupted *UBA4* in the genome of our wild-type (WT) isolate Guy11 by homologous recombination using ILV1 as a selectable marker conferring sulphonyl urea resistance<sup>19</sup>. Three independent Δuba4-carrying mutant strains were recovered, and each had identical phenotypes (Extended Data Fig. 1a-e). One deletant was used to generate the Δuba4 UBA4-GFP complementation strain. On media plates,  $\Delta uba4$  radial growth and sporulation rates were significantly  $(P \le 0.05)$  reduced compared to WT (Extended Data Fig. 1a,b). Reduced radial growth of *M. oryzae* Δ*uba4* mutant strains is consistent with observations in yeast, where tRNA thiolation is required for optimal nutrient sensing and metabolic homeostasis in a biochemical manner independent of protein translation rates<sup>9</sup>. When equal numbers of *M. oryzae* spores were applied to 3-week-old rice seedlings of the susceptible cultivar CO-39, infection with WT and the complementation strain resulted in typical expanded necrotic lesions on leaves by 5 days post inoculation (dpi), but the  $\Delta uba4$  mutant strain produced only pinpoint lesions<sup>20</sup> and was thus non-pathogenic (Fig. 1c, quantified in Fig. 1d). Liquid chromatography-mass spectrometry (LC-MS) analysis of tRNAs from vegetative mycelia showed that, consistent with yeast mutants<sup>16</sup>, both the *M. oryzae*  $\Delta uba4$  mutant strain and an  $\Delta urm1$  deletant that we also generated in Guy11, and which was physiologically indistinguishable from Δuba4 (Extended Data Fig. 1f-k), were abolished for the mcm<sup>5</sup>s<sup>2</sup>U tRNA modification (Fig. 1e; raw values with replicates in Supplementary Table 1) but not for the mcm<sup>5</sup>U tRNA modification (Supplementary Table 1), compared to WT. Like in yeast, M. oryzae Uba4-GFP localized to the fungal cytoplasm (Extended Data Fig. 2). Taken together, we conclude that M. oryzae UBA4 and URM1 are required for optimal axenic growth and sporulation, rice plant infection and cytoplasmic tRNA anticodon U<sub>34</sub> thiolation.

Following adhesion to host leaf surfaces, *M. oryzae* spores germinate, and each form specialized dome-shaped infection structures (appressoria); appressoria penetrate the host cuticle under enormous turgor at 24 h post inoculation (hpi)<sup>21,22</sup> and elaborate bulbous, branching invasive hyphae (IH) that fill the first infected living rice cell by 44–48 hpi before migrating to neighbouring cells<sup>23</sup>. Live-cell imaging of optically clear detached rice leaf sheath epidermal cells showed that *UBA4* was not required for leaf cuticle penetration by appressoria (Extended Data Fig. 1c,d) or for initial IH elaboration after penetration (Fig. 1f) but was essential for filling the first infected rice epidermal cell with IH and for extensive IH spread to neighbouring cells (Fig. 1f and Extended Data Fig. 1e). Similar results were obtained for Δ*urm1* (Extended Data Fig. 1i–k). Thus, *UBA4* and *URM1* are required for extended *M. oryzae* biotrophic growth in living host rice cells.

# $Loss \ of \ \textit{UBA4} \ abolishes \ Pwl 2 \ effector \ accumulation \ in \ the \ biotrophic interfacial \ complex$

During the biotrophic growth phase of rice cell infection, *M. oryzae* IH are separated from host cytoplasm by an extended interfacial zone comprising host-derived membranes  $^{24,25}$ . To better understand the role of *UBA4* in biotrophy, we hypothesized that the biotrophic interfacial compartments separating IH from plant host cytoplasm would be perturbed in  $\Delta uba4$  compared to WT, as was observed previously for another biotrophic growth mutant  $^{25}$ . WT IH are wrapped in the plant host-derived extra-invasive hyphal membrane  $^{14,23}$ , forming a matrix into which apoplastic effectors like Bas4 are secreted via the

conventional ER-Golgi pathway. A focal, plant lipid-rich membrane structure, the biotrophic interfacial complex (BIC), forms an additional compartment, outside IH, in the first infected rice cell and at the tips of IH spreading to adjacent cells<sup>14,26</sup>. Cytoplasmic effectors like Pwl2 (which confers host species specificity) and AVR-Pita (which confers avirulence on rice lines carrying the corresponding Pita R gene) are secreted into the BIC by an unconventional protein secretion pathway before being translocated into the host cell<sup>24</sup>. Effector genes are only expressed in planta, and therefore fluorescently labelled effectors are cellular probes to monitor both effector deployment and biotrophic interfacial membrane integrity<sup>25</sup>. Using the pBV591 vector<sup>26</sup>, we generated a \( \Delta uba4 \) mutant strain producing, under native promoters, Pwl2 fused to mCherry (which also carries an added C-terminal nuclear localization signal (NLS) to concentrate Pwl2 in the rice nucleus and thus confirm secretion into the host cell<sup>24</sup>) and Bas4 fused to green fluorescent protein (GFP). Like our previously generated PWL2-mCherry:NLS and BAS4-GFP-expressing control strain<sup>27</sup>, we found that at 36 hpi, Bas4-GFP correctly outlined \(\Delta uba4\) IH (Fig. 1g) indicating, contrary to our expectations, that the extra-invasive hyphal membrane was not eroded in  $\Delta uba4$ and the apoplast was intact. However, whereas Pwl2-mCherry:NLS accumulated in UBA4+ control BICs and in the nuclei of UBA4+-infected rice cells by 36 hpi (Fig. 1g), in contrast, Pwl2-mCherry:NLS was not visible in  $\Delta uba4$  IH or associated rice nuclei (Fig. 1g). Together, these initial results suggested that UBA4 was required for Pwl2 production and/or secretion and accumulation in the BIC, and also possibly for BIC integrity, but was not required for Bas4 production and secretion or for apoplastic space integrity.

#### PWL2 mRNA translation requires U<sub>34</sub> thiolation

We initially considered that the loss of Pwl2 secretion and accumulation in  $\Delta uba4$  BICs indicated BIC integrity (but not apoplastic integrity) was disrupted in  $\Delta uba4$ . However, closer inspection revealed  $\Delta uba4$ BICs by bright-field microscopy and, like for UBA4+ (and as reported by others), Bas4-GFP visibly accumulated under Δuba4 BICs (Fig. 2a). Thus, UBA4 is not required for BIC formation but is required for Pwl2-mCherry: NLS accumulation in BICs. Similarly, a strain expressing Pwl2-GFP and Bas4-mCherry:NLS, constructed to ensure that the defect in Pwl2 BIC accumulation in  $\Delta uba4$  was not due to the fluorescent tag, showed Bas4-mCherry: NLS was secreted into the Δuba4 apoplast and accumulated under the BIC, but Pwl2-GFP was not detected in any Δuba4-infected cells (Extended Data Fig. 3). To understand why Pwl2 did not accumulate in Δuba4 BICs, we considered that in yeast, tRNA anticodon wobble U<sub>34</sub> thiolation by Uba4 prevents ribosome pausing and protein aggregation by improving the efficiency of AA-ending cognate codon decoding<sup>7,17</sup>. We thus hypothesized that the loss of Pwl2 secretion and accumulation in Δuba4 BICs indicated PWL2-mCherry:NLS mRNA (but not BAS4-GFP mRNA) was translationally impaired in planta in the  $M. oryzae \Delta uba4$  mutant strain due to ribosome pausing at AA-ending codons. In yeast, paromomycin treatment mitigates ribosomal pausing at AA-ending codons in U<sub>34</sub> thiolation deficient mutant strains by increasing near-cognate tRNA acceptance. We infused leaf sheaths with 1 mg ml<sup>-1</sup> paromomycin in 0.2% gelatin at 36 hpi and observed the effects at 44 hpi. In the control UBA4+ strain, PWL2-mCherry:NLS mRNA translation and BAS4-GFP mRNA translation were not affected by paromomycin treatment, and both Pwl2-mCherry: NLS and Bas4-GFP were correctly deployed in IH, although, consistent with its role as a protein synthesis inhibitor, UBA4+ IH growth was severely attenuated compared to the untreated control (Extended Data Fig. 4). In  $\Delta uba4$ IH, paromomycin treatment restored Pwl2-mCherry:NLS secretion and accumulation in BICs (Fig. 2b). Furthermore, in the  $\Delta urm1$  mutant strain (which closely resembled Δuba4; Extended Data Fig. 1f-k), we also observed loss of Pwl2-mCherry:NLS accumulation in the Δ*urm1* BIC, and this was similarly (but weakly) remediated by paromomycin treatment (Fig. 2b). Concordant with yeast findings<sup>7</sup>, remediation of Pwl2-mCherry:NLS production by paromomycin suggests that

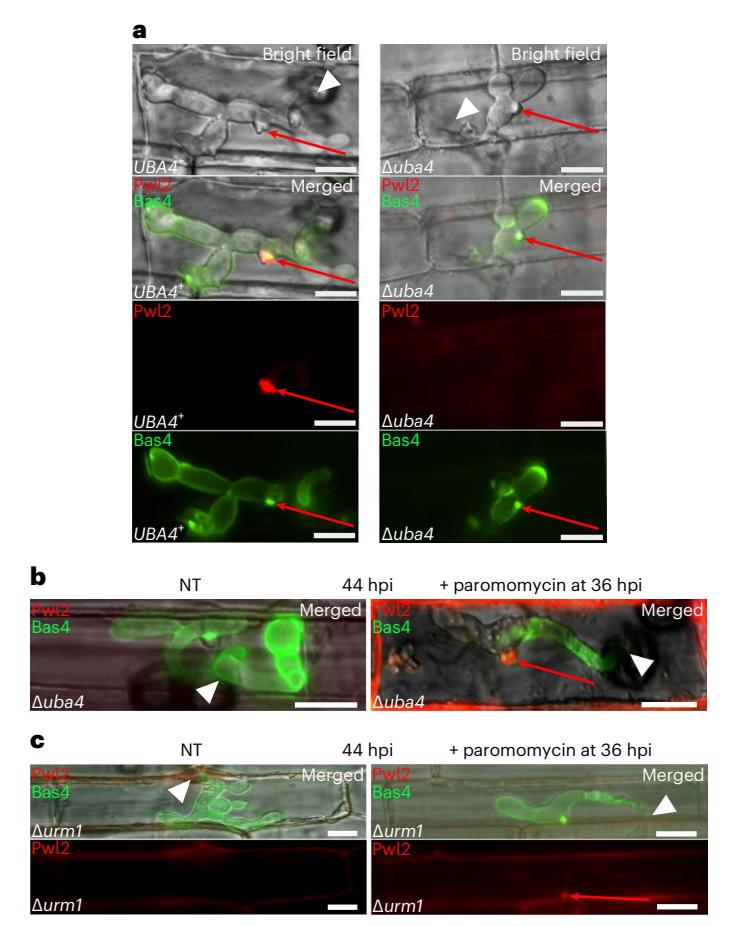


**Fig. 2**| **The tRNA thiolation modification is required for** *PWL2* (**but not** *BAS4*) **mRNA translation. a**, The  $\Delta uba4$  mutant strain is never observed accumulating Pwl2 in BICs. Live-cell images of detached rice leaf sheath epidermal cells were taken at 36 hpi. White arrowheads indicate penetration sites; red arrows indicate visible BICs. Scale bars, 10 μm. **b,c**, Paromomycin treatment of detached rice leaf sheath epidermal cells colonized with  $\Delta uba4$  (**b**) or  $\Delta urm1$  (**c**) mutant strains at 36 hpi restored Pwl2 translation and secretion into the BIC by 44 hpi in 100% of treated cells. Pwl2-mCherry fluorescence was weak following paromomycin treatment, and the required increase in signal intensity revealed autofluorescence in host rice cell walls. White arrowheads indicate penetration sites; red arrows indicate visible BICs. Scale bars, 10 μm. NT, no treatment. In **a-c**, calculations and representative images are based on the observations of 50 infected rice cells per leaf sheath per treatment, repeated in triplicate.

ribosomal pausing is occurring in both the  $\Delta uba4$  and  $\Delta urm1$  mutant strains, likely due to inefficient decoding of AA-ending cognate codons, leading to the loss of PWL2-mCherry:NLS mRNA translation. We conclude that the M. oryzae Uba4–Urm1 sulfur relay system is required for  $s^2U_{34}$  tRNA modification-dependent efficient codon decoding of PWL2-mCherry:NLS mRNA (but not BAS4-GFP mRNA) in planta.

#### AVR-Pita secretion requires U<sub>34</sub> thiolation

We next asked whether tRNA thiolation was only required for PWL2 mRNA translation or whether it was required for other unconventionally secreted cytoplasmic effectors that accumulate in the BIC, of which few are experimentally determined, including AVR-Pita<sup>26</sup>. To address this, we generated  $\Delta uba4$  and  $UBA4^+$  strains expressing BAS4-GFP along with AVR-Pita-mCherry:NLS expressed under its native promoter. Figure 3 shows that AVR-Pita-mCherry:NLS weakly accumulated in  $UBA4^+$  BICs compared to Pwl2-mCherry:NLS, as previously described<sup>26</sup>. However, no AVR-Pita-mCherry:NLS protein accumulation was observed in  $\Delta uba4$  BICs unless  $\Delta uba4$ -infected rice cells were treated with paromomycin

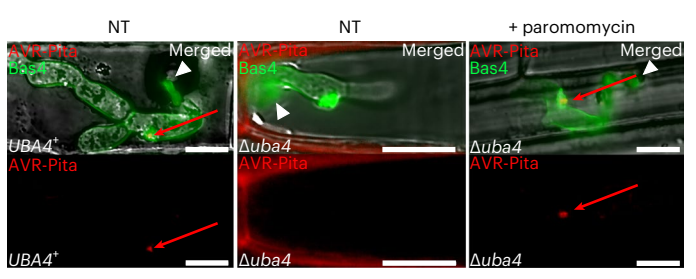


Fig. 3 | Translation of the unconventionally secreted AVR-Pita effector requires tRNA thiolation. Live cell imaging at 44 hpi of detached rice leaf sheath epidermal cells shows that in 100% of observed cells, AVR-Pita was secreted into the  $UBA4^+$  BIC, but in the  $\Delta uba4$  strain, the accumulation of AVR-Pita in BICs was abolished unless cells were treated with paromomycin at 36 hpi. Calculations and representative images are based on the observations of 50 infected rice cells per leaf sheath per treatment, repeated in triplicate. White arrowheads indicate penetration sites; red arrows indicate AVR-Pita in BICs. Scale bars, 10  $\mu$ m. For the  $\Delta uba4$  NT panel, the red channel signal intensity was increased to confirm that AVR-Pita was not accumulating in the BIC, revealing autofluorescence in the host rice cell wall.

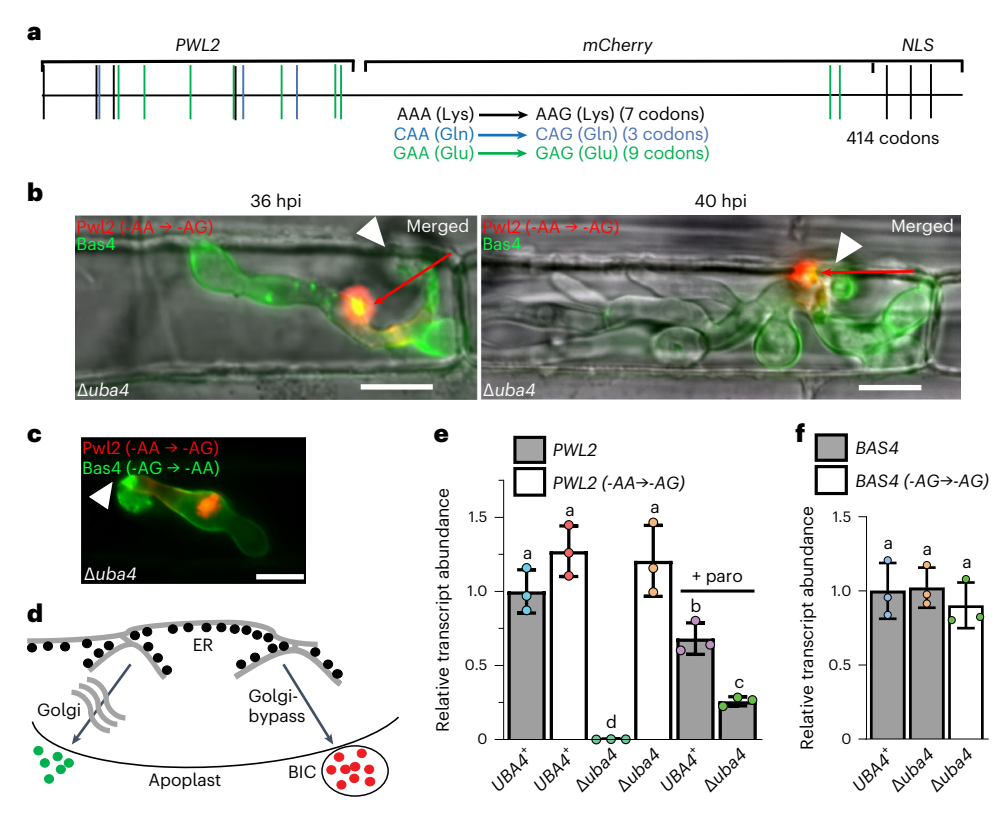
(Fig. 3). In contrast, the experimentally determined apoplastic effector  $Slp1^{28}$  was, like Bas4, successfully produced and secreted into the apoplast by a  $\Delta uba4$  strain expressing SLP-GFP under its native promoter (Extended Data Fig. 5). Therefore, Uba4–Urm1-dependent tRNA wobble  $U_{34}$  thiolation is required for the translation of mRNAs encoding at least two unconventionally secreted cytoplasmic effectors but not for the translation of mRNAs encoding at least two ER–Golgi secreted apoplastic effectors.

# $Synonymous\,codon\,recoding\,remediates\,PWL2\,mRNA\\translation$

To confirm that the loss of PWL2 and AVR-Pita (but not BAS4 or SLP1) mRNA translation was due to inefficient decoding of AA-ending cognate codons following the loss of tRNA thiolation, we reasoned that recoding AA-ending codons to synonymous AG-ending codons carrying guanine in the third position (which do not require the s<sup>2</sup>U<sub>34</sub> modification for decoding<sup>3,17</sup>) would remediate cytoplasmic effector mRNA translation and unconventional secretion in the absence of tRNA wobble  $U_{34}$  thiolation. To test this, we generated a  $\Delta uba4$  strain expressing BAS4-GFP along with a recoded form of PWL2-mCherry:NLS (hereafter termed PWL2 (-AA $\rightarrow$  -AG)) where all AA-ending codons were recoded to synonymous AG-ending codons (Fig. 4a and Extended Data Fig. 6). Expressing  $PWL2(-AA \rightarrow -AG)$  in  $\Delta uba4$  fully remediated Pwl2 production and its secretion and accumulation in the  $\Delta uba4$  BIC (Fig. 4b). In some cases, expressing  $PWL2(-AA \rightarrow -AG)$  resulted in large and/ or unstable Δuba4 BICs (Extended Data Fig. 7). We conclude that during host infection, because  $PWL2(-AA \rightarrow -AG)$  mRNA is under the same promoter and encodes the same amino acid sequence as PWL2-mCherry:NLS, then the translation of native PWL2 mRNA (encoding an unconventionally secreted effector) must require tRNA wobble U<sub>34</sub> thiolation-dependent efficient decoding of AA-ending cognate codons.

#### BAS4 translation is unaffected by AA-ending codon recoding

To better understand why *BAS4* but not *PWL2* mRNAs are translated in  $\Delta uba4$ , we next expressed in  $\Delta uba4$  a version of *BAS4-GFP* where all AG-ending codons were recoded to synonymous AA-ending codons (Extended Data Fig. 8a), hereafter *BAS4(-AG \rightarrow -AA)*, along with *PWL2 (-AA \rightarrow -AG)* as a positive control for protein translation, with the expectation that *BAS4(-AG \rightarrow -AA)* mRNAs would not be translated in  $\Delta uba4$ . However, in contrast to native *PWL2* mRNA, which was not translated in  $\Delta uba4$  unless all AA-ending codons were recoded to synonymous AG-ending codons, the recoding of all AG-ending codons in *BAS4-GFP* 



 $Fig. 4 \,|\, Unconventional\, protein\, secretion\, but\, not\, conventional\, ER-Golgi\, secretion\, in\, host\, cells\, is\, AA-ending\, codon\, decoding-dependent.\, a,$ 

Synonymous codon changes in *PWL2-mCherry:NLS* to yield *PWL2(-AA) -AG)*. **b**, Live-cell imaging at 36 hpi and 40 hpi of detached rice leaf sheath epidermal cells infected with  $\Delta uba4$  shows *PWL2* mRNA translation was remediated in 100% of infected cells by synonymous codon recoding. **c**, In 100% of observed cells, synonymous AG-ending to AA-ending codon changes in *BAS4-GFP* did not affect Bas4-GFP secretion in  $\Delta uba4$ . Images were taken at 36 hpi. In **b** and **c**, white arrowheads indicate penetration sites; red arrows indicate BICs. Scale bars, 10 µm. Calculations and representative images are based on the observations of 50 infected rice cells per leaf sheath per treatment, repeated in triplicate. **d**, Unconventionally secreted effectors requiring tRNA wobble U<sub>34</sub> thiolation carry signal peptides and are likely secreted through the Golgi-bypass pathway<sup>29</sup>. **e**, Using *mCherry*-specific primers, qPCR analysis of cDNAs obtained at 42 hpi from detached rice leaf sheaths infected with the indicated strains shows that *PWL2* 

mRNA abundance is codon decoding-dependent. Paro is treatment with 1 mg ml<sup>-1</sup> paromomycin in 0.2% gelatin. Values are the means  $\pm$  s.d.; n=3 biological replicates. Different letters above bars indicate significant differences at  $P \le 0.05$  (Student–Newman–Keuls test). **f**, Using *GFP*-specific primers, qPCR analysis of cDNAs obtained at 42 hpi from detached rice leaf sheaths infected with the indicated strains shows that *BAS4* mRNA abundance is not codon decoding-dependent. Values are the means  $\pm$  s.d.; n=3 biological replicates. Same letters above bars indicate no significant differences at  $P \le 0.05$  (Tukey's HSD of one-way ANOVA). In **e** and **f**, values were calculated for each strain by normalizing the expression of *PWL2-mCherry:NLS*, *PWL2* (- $AA \rightarrow -AG$ ), *BAS4-GFP* and *BAS4* (- $AG \rightarrow -AA$ ) against the *M. oryzae* actin-encoding gene *MoACT*, then normalizing these values against either the relative transcript abundance of *PWL2-mCherry:NLS* in untreated *UBA4*<sup>+</sup> for *PWL2-mCherry:NLS* and *PWL2* (- $AA \rightarrow -AG$ ) or against *BAS4-GFP* in *UBA4*<sup>+</sup> for *BAS4-GFP* and *BAS4* (- $AG \rightarrow -AA$ ). Exact *P* values are given in Source Data Extended Data Fig. 4.

to synonymous AA-ending codons did not, as hypothesized, abolish Bas4 secretion into the  $\Delta uba4$  apoplast (Fig. 4c; more examples shown in Extended Data Fig. 8b). Thus, the  $s^2U_{34}$  tRNA modification is not required for translating conventional ER–Golgi-secreted  $BAS4(\cdot AG \rightarrow \cdot AA)$  mRNAs, although we cannot rule out that some changes to translation speed may occur. In M. oryzae, both apoplastic and cytoplasmic effectors carry signal peptide sequences targeting them for synthesis on rough ER, but cytoplasmic effectors are then likely secreted via the type IV unconventional secretion pathway, which bypasses the Golgi apparatus<sup>29</sup> (Fig. 4d). Our results suggest that the  $s^2U_{34}$  tRNA modification and efficient AA-ending codon decoding is required for the folding of newly synthesized peptides in the type IV Golgi-bypass pathway but not in the ER–Golgi network.

#### PWL2 mRNA levels are AA-ending codon decoding-dependent In addition to translational differences between PWL2 and BAS4

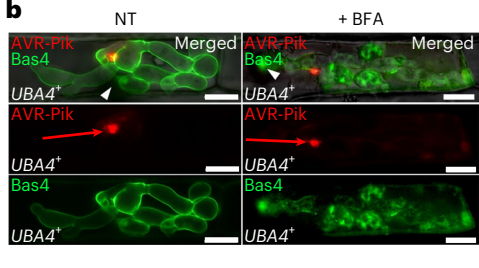
In addition to translational differences between PWL2 and BAS4 mRNAs, differences in transcript stability were gleaned from quantitative real-time PCR (qPCR). Using mCherry-specific primers, we found that, compared to PWL2-mCherry:NLS expression in  $UBA4^+$  IH, PWL2-mCherry:NLS transcripts were barely detected in  $\Delta uba4$  IH.

However, recoded PWL2 (- $AA \rightarrow -AG$ ) expression levels in both  $UBA4^+$  and  $\Delta uba4$  IH were indistinguishable from native PWL2 expression levels in  $UBA4^+$ , while paromomycin treatment partially remediated PWL2-mCherry:NLS expression levels in  $\Delta uba4$  (Fig. 4e). In contrast, using GFP-specific primers, we found that BAS4-GFP expression levels, including of the recoded  $BAS4(-AG \rightarrow -AA)$  version, were not affected in  $\Delta uba4$  IH compared to  $UBA4^+$  (Fig. 4f). Thus, PWL2 mRNA stability but not BAS4 mRNA stability in M. oryzae IH is dependent on the efficient decoding of AA-ending cognate codons by  $s^2U_{34}$ -modified tRNAs.

# Cytoplasmic effector mRNAs are enriched in AA-ending codons

To better understand the dependency of *PWL2* and *AVR-Pita* mRNA translation (but not *BAS4* or *SLP1* mRNA translation) on Uba4-dependent tRNA wobble U<sub>34</sub> thiolation, we next asked whether AA-ending codon usage was biased or unbiased in cytoplasmic effector mRNAs compared to apoplastic effector mRNAs. To address this, we analysed AA- and synonymous AG-ending codon usage in all *M. oryzae* protein coding sequences as well as in *PWL2*, *AVR-Pita*, *BAS4* and *SLP1* mRNAs (Extended Data Fig. 9a). We also examined mRNAs encoding proteins

а			
Apoplasti	c effectors	Cytoplasm	ic effectors
mRNAs	AA-ending codon usage rate	mRNAs	AA-ending codon usage rate
ΣCDS	29%	PWL2	67%
BAS4	17%	AVR-Pita	88%
SLP1	7%	BAS1	64%
BAS113	20%	BAS107	52%
AVR1-CO39*	44%	AvrPiz-t*	50%
TOXB*	42%	AVR-Pik*	92%
* = MAX	effector	AVR-Pia*	80%



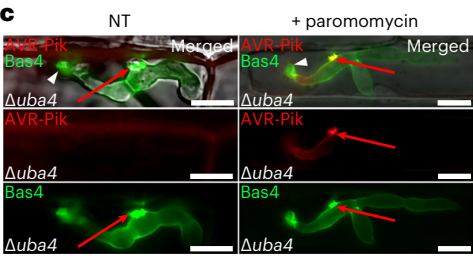


Fig. 5 | Unconventionally secreted cytoplasmic effector mRNAs are AA-ending codon-rich. a, Cytoplasmic effector mRNAs are enriched for AA-ending codons relative to synonymous AG-ending codons, whereas apoplastic effector mRNA codon usage, and codon usage from across all 12,936 protein coding sequences in the *M. oryzae* genome ( $\Sigma$ CDS), is biased towards AG-ending codons. mRNA AA-ending codon usage rates are calculated using the codon counts in Extended Data Fig. 9a-c and are given as the fraction of AA-ending codons as a percentage of the total number of AA- and synonymous AG-ending codons. **b**, Live-cell imaging of a *UBA4*<sup>+</sup> strain expressing AVR-PIK-mCherry:NLS and Bas4-GFP treated with BFA, which inhibits conventional ER-Golgi secretion, shows that AVR-Pik is secreted into the BIC via the unconventional protein secretion pathway. Infected detached rice leaf sheath epidermal cells were treated at 36 hpi with 50 μg ml<sup>-1</sup>BFA for 4 h before observation. Blocked ER-Golgi secretion in BFA-treated samples resulted in Bas4 retention in IH, but AVR-Pik secretion into BICs was unaffected. c, Live-cell imaging of detached rice leaf sheath epidermal cells infected with a  $\Delta uba4$  strain expressing AVR-PIK-mCherry:NLS and Bas4-GFP shows that AVR-Pik is produced and secreted into the BIC in a Uba4-mediated, codon decoding-dependent manner. AVR-Pik was not detected in any untreated  $\Delta uba4$ -infected rice cells. Infected cells treated with 1 mg ml<sup>-1</sup> paromomycin at 36 hpi and viewed at 44 hpi showed remediated AVR-Pik translation and secretion into the Δuba4 BIC in all observed cells. In **b** and **c**, white arrowheads indicate penetration sites; red arrows indicate BICs. Scale bars, 10 µm. Calculations and representative images are based on the observations of 50 infected rice cells per leaf sheath per treatment, repeated in triplicate.

with stringent evidence for BIC accumulation (AvrPiz-t, Bas1 and Bas107)<sup>24,26,30</sup>, confirmed brefeldin A (BFA)-insensitive unconventional secretion (Bas1 and Bas107)<sup>24</sup> and confirmed BFA-sensitive conventional ER–Golgi secretion (Bas113)<sup>24</sup> (Extended Data Fig. 9b). By calculating the AA-ending codon usage rate (that is, the fraction of AA-ending codons as a percentage of the total number of AA- and synonymous AG-ending codons), we found that cytoplasmic effector mRNAs were enriched for AA-ending codons relative to synonymous AG-ending codons whereas in contrast, apoplastic effector mRNA codon usage,

like codon usage across all *M. oryzae* protein coding sequences, was biased against AA-ending codons in favour of AG-ending codons (Fig. 5a; underlying codon data in Extended Data Fig. 9a-c). This suggests cytoplasmic effector mRNA codon usage is under selection for AA-ending codon enrichment while apoplastic effector mRNA codon usage, like genome-wide codon usage, is not.

AvrPiz-t is a MAX (*Magnaporthe oryzae* avirulence and ToxB-like) effector, a class of sequence-unrelated but structurally conserved fungal effectors that also includes AVR-Pik, Avr-Pia and Avr1-CO39 from *M. oryzae* and ToxB from the wheat pathogen *Pyrenophora tritici-repentis*<sup>31–33</sup> (Extended Data Fig. 9c). Transient expression studies in rice protoplasts<sup>34</sup> suggest AVR-Pik and AVR-Pia are cytoplasmic MAX effectors<sup>32</sup>, while *M. oryzae* AVR1-CO39 and *P. tritici-repentis* ToxB are apoplastic MAX effectors<sup>32,35</sup>. Figure 5a shows that despite protein structural conservation, AA-ending codon usage rates are higher for *AVR-Pik* and *AVR1-Pia* mRNAs than for *AVR1-CO39* mRNAs and *P. tritici-repentis TOXB* mRNAs. Thus, cytoplasmic MAX effector mRNAs are enriched for AA-ending codons, whereas apoplastic MAX effector mRNAs across species are depleted for AA-ending codons relative to synonymous AG-ending codons (Fig. 5a and Extended Data Fig. 9c).

Based on the 92% AA-ending codon usage rate for AVR-Pik mRNAs (Fig. 5a), we predicted that AVR-Pik was secreted into the BIC via the unconventional protein secretion pathway in a tRNA wobble U<sub>34</sub> thiolation-dependent manner. By expressing  $AVR\text{-}Pik\text{-}mCherry:NLS}$  and BAS4-GFP, Fig. 5b shows how, in  $UBA4^+$ , BFA treatment, which inhibits conventional ER-to-Golgi secretion, prevented Bas4 secretion (which is retained in IH) but did not affect AVR-Pik accumulation in the BIC, confirming AVR-Pik is unconventionally secreted. Figure 5c shows that in  $\Delta uba4$  mutant strains, AVR-Pik was not produced and secreted into the BIC unless infected cells were treated with paromomycin. Thus, as predicted from AA-ending codon usage rates, AVR-Pik is produced and secreted into the BIC via the unconventional protein secretion pathway in an AA-ending codon decoding-dependent manner.

#### Codon usage tunes Pwl2 secretion to foster BIC stability

We next asked, why would M. oryzae evolve AA-ending codons in PWL2 mRNA—whose efficient decoding requires tRNA thiolation by the multi-step Uba4-Urm1 sulfur relay system—when a strain lacking UBA4 can translate PWL2 mRNAs carrying all AG-ending synonymous codons instead? To address this, we expressed  $PWL2(-AA \rightarrow -AG)$ , along with BAS4-GFP, in the UBA4<sup>+</sup> WT strain, Figure 6a shows that, relative to the PWL2-mCherry:NLS-expressing control strain, the expression of PWL2 (-AA $\rightarrow$  -AG) resulted in the formation of giant, brightly fluorescing BICs that were unstable and often either split or elongated rather than spherical. Note that Pwl2 (-AA→ -AG) accumulated in rice nuclei, indicating that the protein was correctly folded and translocated into the host cell. BICs were also visualized by brightfield and were obviously increased in size in the *UBA4*<sup>+</sup> strain expressing recoded  $PWL2(-AA \rightarrow -AG)$  compared to the  $UBA4^+$  strain expressing native PWL2(Fig. 6a). Pwl2 (-AA→ -AG) accumulated in expanded and fragmented BICs following BFA treatment, which blocks the secretion of apoplastic (but not cytoplasmic) effectors through the conventional ER-Golgi pathway<sup>24</sup>, indicating recoded Pwl2 continued to be trafficked via the unconventional protein secretion pathway and did not spill into the ER-Golgi network (Extended Data Fig. 10). Considering PWL2 (-AA → -AG) transcript abundance in UBA4<sup>+</sup> was not significantly different to native PWL2 mRNA levels (Fig. 4e), these data together suggest recoding AA-ending codons to synonymous AG-ending codons in the UBA4<sup>+</sup> background leads to unregulated PWL2(-AA→-AG) mRNA translation resulting in Pwl2 (-AA→ -AG) protein overproduction and super-secretion into the BIC. Inoculating susceptible rice plants with spores of the *UBA4*<sup>+</sup> strain expressing *PWL2* (- $AA \rightarrow -AG$ ) resulted in fewer and smaller disease lesions compared to leaves inoculated with the UBA4+ strain expressing native PWL2 (Fig. 6b,c), indicating that giant, unstable BICs resulting from recoded Pwl2 super-secretion are

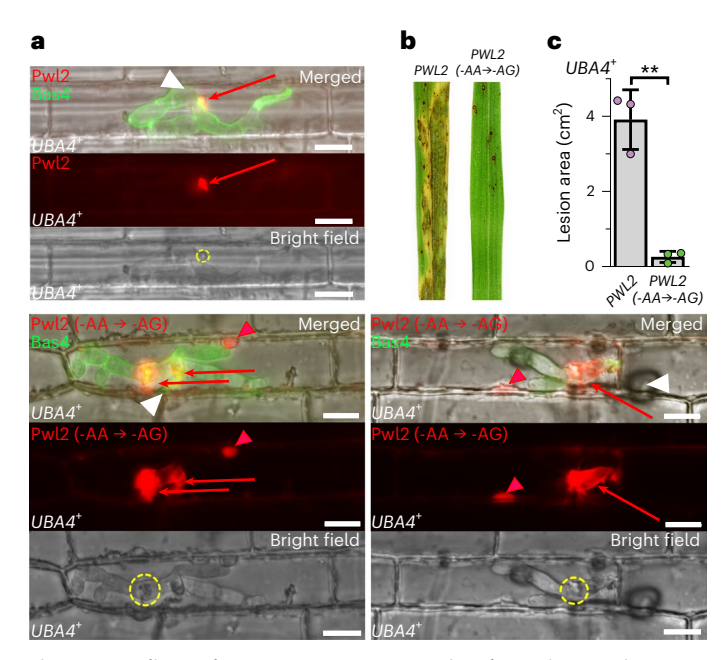


Fig. 6 | AA-ending codon usage tunes unconventional protein secretion in living host cells. a, Live-cell imaging at 38 hpi of detached rice leaf sheath epidermal cells infected with the indicated strains shows that, compared to the PWL2-mCherry:NLS-expressing UBA4+ control strain (top left), expressing  $PWL2(-AA \rightarrow -AG)$  in  $UBA4^+$  resulted in recoded Pwl2 super-secretion into BICs. which are destabilized (two examples shown at bottom left and right). Hatched yellow circles indicate BIC sizes, which are expanded in IH expressing recoded PWL2 compared to those expressing native PWL2. White arrowheads indicate penetration sites; red arrows indicate Pwl2 or recoded Pwl2 in BICs; red arrowheads indicate recoded Pwl2 in host nuclei. Scale bars, 10 um. One hundred per cent of infected rice cells displayed the phenotypes shown. Representative images are based on the observations of 50 infected rice cells per leaf sheath per treatment, repeated in triplicate. **b**, Spores of UBA4+ expressing BAS4-GFP along with native PWL2 (fused to mCherry:NLS) or recoded PWL2 (-AA $\rightarrow$  -AG) were applied to 3-week-old seedlings of the susceptible rice cultivar CO-39 at a rate of 1 × 10<sup>5</sup> spores per ml. Leaves were imaged at 5 dpi. Images are representative of at least five leaves from three biological replicates. c, Sections of 10 cm length of infected leaves at 5 dpi were imaged, and the disease lesion areas were quantified using Image J. Values are the means  $\pm$  s.d. of three biological replicates. Areas were analysed by the two-tailed unpaired t-test. \*\*Statistically significant differences (P < 0.05). P = 0.013 between strains UBA4+PWL2-mCherry:NLS BAS4-GFP and UBA4+ PWL2 (-AA+ -AG) BAS4-GFP.

detrimental to infection; thus, cytoplasmic effector codon usage may influence M. oryzae fitness in the field. We conclude that AA-ending codon usage in PWL2 mRNA modulates translation to precisely tune Pwl2 production and optimize rates of unconventional protein secretion into the BIC. In doing so, tRNA wobble  $U_{34}$  thiolation and codon usage bias directly contribute to M. oryzae BIC integrity and facilitate biotrophic growth in living rice cells.

#### Discussion

To subvert host cell innate immunity, animal and plant microbial pathogens secrete effector proteins and virulence factors<sup>36</sup>, often via unconventional pathways<sup>24,29,37,38</sup> whose molecular underpinnings are only starting to emerge<sup>29</sup>. tRNA wobble U<sub>34</sub> thiolation is required for efficient decoding of AA-ending cognate codons to prevent transient ribosomal pausing, which affects protein folding<sup>7</sup> and protein homeostasis<sup>17</sup>. However, U<sub>34</sub> thiolation mutants have minor translational defects<sup>9</sup>, and specific biological roles for this universal modification are poorly understood. Here we describe a physiological role for tRNA U<sub>34</sub> thiolation in tuning unconventional but not conventional

protein secretion and show how such tuning is essential for fungal virulence

In our study, the loss of tRNA thiolation eliminated unconventional protein secretion due to ribosomal pausing at AA-ending codons, which prevented protein translation and secretion, whereas expressing recoded PWL2 mRNA carrying all AG-ending codons caused unregulated PWL2 mRNA translation and Pwl2 super-secretion that gave rise to giant, unstable BICs and the loss of fungal virulence. Thus, efficient AA-ending codon decoding by tRNA wobble s<sup>2</sup>U<sub>34</sub> anticodons tunes the translation of cytoplasmic effector mRNAs, which carry more AA-ending codons than apoplastic mRNAs, in order to control the rate of unconventional cytoplasmic effector secretion and maintain BIC stability. In contrast, ribosomal pausing on the relatively small number of AA-ending codons carried by native BAS4 and SLP1 mRNAs (2 and 1. respectively) did not prevent peptide synthesis, nor, counterintuitively, did changing all AG-ending codons to AA-ending codons in recoded BAS4 (to give a total of 12 AA-ending codons in BAS4(-AG $\rightarrow$  -AA), comparable to the 14 AA-ending codons in native PWL2). Why is efficient AA-ending codon decoding necessary for cytoplasmic but not apoplastic effector mRNA translation and protein secretion? Although counterintuitive, our results are consistent with findings in yeast, where the integrity of ER-Golgi proteins was less affected by changes in decoding speeds arising from the loss of the s<sup>2</sup>U<sub>34</sub> modification than cytosolic proteins due to different co-translational mechanisms and folding constraints across the ER membrane compared to the cytoplasm<sup>7</sup>. We suggest that similarly, our results showing the different outcomes of *PWL2* and *BAS4(-AG\rightarrow-AA)* mRNA translation in  $\triangle uba4$  may be consistent with the notion that proteins secreted unconventionally through the type IV Golgi-bypass pathway are subjected to different co-translational mechanisms and protein folding constraints compared to conventional ER-Golgi secreted proteins. Consequently, the unconventional protein secretion pathway (but not the conventional ER-Golgi network) is intolerant of ribosome pausing and changes to mRNA translation speeds resulting from inefficient AA-ending codon decoding, which may cause misfolding and elimination of newly synthesized peptides<sup>7</sup>. When considering that local translation elongation rates are tightly controlled by individual codons<sup>39</sup>, and that intragenic codon frequency bias leads to variable ribosome decoding speeds along mRNAs to optimize co-translational protein folding and protein translocation across membranes<sup>40</sup>, it is conceivable that unconventionally secreted effector protein mRNAs (but not apoplastic effector mRNAs) may evolve AA-ending codon-enriched mRNAs precisely in order for nascent peptides to be translated at speeds that optimize protein folding and secretion through the type IV Golgi-bypass pathway, which is the only known means of targeting effector proteins to BICs for entry into host rice cells. For sequence-unrelated but structurally conserved MAX effectors, this suggests cytoplasmic MAX effectors may be under dual selection for both sequence-unrelated structural conservation and AA-ending codon usage frequency. Indeed, AA-ending codon usage rates successfully predicted an unconventionally secreted cytoplasmic MAX effector, AVR-Pik, from among MAX effectors that shared sequence-unrelated structural folds. AA-ending codon usage rates could thus be used to complement other efforts to identify new effectors, such as those involving proteomics or structural approaches<sup>41</sup>, although functional confirmation will still be necessary.

The codon-decoding dependency of *PWL2* but not *BAS4* mRNA stability provides additional evidence for the notion that ribosomal pausing affects the translation of cytoplasmic but not apoplastic effector proteins due to differences in co-translational and protein folding microenvironments. To maintain protein homeostasis, protein quality control pathways that detect stalled or slowed and colliding ribosomes during elongation trigger mRNA decay as well as the degradation of nascent peptides <sup>42–44</sup>. Following ribosome collision detection by the E3 ubiquitin ligase Znf598 (Hel2 in yeast <sup>42</sup>), and in coordination with aberrant protein degradation, non-functional ribosome-associated mRNAs

are eliminated via a quality control pathway called the No-Go Decay (NGD) mRNA surveillance pathway. During NGD, aberrant mRNAs undergo endonucleolytic cleavage and degradation to release stalled ribosomes 42.45-47. PWL2 mRNA decay and undetectable Pwl2 protein production (and their reversal by codon recoding or paromomycin treatment) suggest a similar response to ribosomal pausing at AA-ending codons in M. oryzae. Tightly linking mRNA stability with protein quality control may, along with translational speed control, provide an additional layer of cytoplasmic effector production fine-tuning. Indeed, one could speculate that NGD may underpin the in planta-specific expression of fungal effector genes. Thus, future studies directed at understanding the coupling of ribosome pausing at AA-ending codons with nascent protein degradation and NGD, and their connections to secretion, are warranted.

Uncovering an effector mRNA codon usage code<sup>48</sup> that may adapt translation elongation speeds to co-translational protein folding constraints in the type IV Golgi-bypass pathway could help identify new effectors secreted by unconventional routes not just in *M. oryzae* but also in other plant pathogenic fungi and oomycetes that use this alternative effector secretion route<sup>37,41</sup>, thereby facilitating the search for novel sources of durable plant host resistance. In addition, parasitic protists including *Leishmania* and the malaria parasite *Plasmodium* traffic virulence factors by unconventional secretion pathways<sup>38</sup>. Our results may aid in deciphering the poorly understood rules of cargo selection, sorting and translocation<sup>38</sup> in these harrowing agents of human affliction. Together, we have shed new light on a microbial process central to many challenging plant and human diseases.

#### Methods

#### Strains, culture conditions and physiological analyses

All fungal strains used in this study are listed in Supplementary Table 2. The *M. oryzae* isolate Guy11<sup>11</sup> was used as the parental WT strain. Strains were grown on complete media (CM) plates<sup>22</sup> and were measured and imaged after 10 days growth using a Sony Cyber-shot digital camera (14.1 megapixels). Spores were collected from 10-day-old CM plates and counted on a haemocytometer, repeated in triplicate. Spores for downstream applications were collected from 12- to 14-day-old oatmeal agar plates (1.5% w/v prepared using Oatmeal Agar, Bioworld). For whole-plant inoculations, spores were applied in 0.2% gelatin at a rate of 1 × 10<sup>5</sup> spores per ml to 3-week-old seedlings of the susceptible rice cultivar CO-39. Infected leaves were collected, dried and imaged at 5 dpi. Images are representative of at least five leaves from each of three independently inoculated plants per strain. For disease area calculations, 10 cm sections of infected leaves were used in triplicate and quantified using ImageJ. Appressorial formation and penetration rates, and cell-to-cell movement rates, were determined by inoculating three detached rice leaf sheaths (from three different plants) per strain with  $0.5 \times 10^5$  spores per ml. Leaf sheaths were prepared for microscopy as described previously22.

#### **Strain construction**

UBA4 and URM1 were deleted in the Guy11 WT strain by the PCR-based split-marker method<sup>19</sup> using the primers in Supplementary Table 3. Briefly, the coding region of UBA4 and URM1 was replaced by the ILV1 gene conferring sulphonyl urea resistance. At least three independent deletants per gene were confirmed by PCR and subsequently characterized. One deletant of each gene was used to receive the respective add-back complementation vector carrying UBA4 or URM1 fused to GFP, vectors carrying PWL2-mCherry:NLS and BAS4-GFP, and, for Δuba4, codon recoded versions of these genes or the other effector genes described in the text.

#### LC-MS-based tRNA modification detection

LC-MS-based tRNA modification detection <sup>49,50</sup> was performed by Arraystar on tRNAs of the indicated strains that were separated from total small RNAs extracted from vegetative hyphae cultured in liquid CM culture for 42 h. Three biological replicates of each strain were used for the following tRNA modification analysis. After extensive washing with distilled H<sub>2</sub>O, mycelia were homogenized in liquid nitrogen, and total RNAs were extracted using the TRIzol reagent (Invitrogen), according to the manufacturer's standard procedure. The prepared total RNAs were then subjected to small RNA isolation using the PureLink microRNA Isolation Kit (Invitrogen) by following the manufacture's instruction manual. Small RNA quality was estimated by running on a denatured agarose gel, and the RNA quantity was measured using a Nanodrop Spectrophotometer. More than 10 µg of small RNAs per biological replicate were provided to Arraystar for further tRNA isolation and modification analysis. There, tRNAs were isolated from small RNAs by 7.5% PAGE (29:1 acrylamide: bisacrylamide) containing 7 M urea. The 60-90 nt band of tRNA was excised from the gel, extracted with 0.3 M NH4Ac and precipitated with glycogen and ethanol, then quantified using the Qubit RNA HS Assay kit (ThermoFisher). Purified tRNA was hydrolysed to single, dephosphorylated nucleosides in a 50  $\mu$ L reaction volume containing 10 U benzonase (Sigma), 0.1 U phosphodiesterase I (US Biological) and 1 U alkaline phosphatase (NEB) following incubation at 37 °C for 3 h. The hydrolysed nucleoside solution was deproteinized using a Satorius 10,000 Da molecular weight cut-off spin filter. The mononucleoside analytes were then separated on an Agilent Zobax SB-Aq liquid chromatography column with flow rate determined by a solvent gradient generated from mixing solution A (0.1% (vol/vol) final concentration of formic acid in HPLC-grade water) and solution B (0.1% (vol/vol) final concentration of formic acid in 100% acetonitrile). tRNA modifications including mcm<sup>5</sup>s<sup>2</sup>U and mcm<sup>5</sup>U were identified by an Agilent 6460 Triple Quadrupole mass analyser running in multiple reaction monitoring (MRM) mode at the parent to daughter ion transition of  $(m/z 333.0 \rightarrow 201.0)$ . LC-MS data were acquired using Agilent Qualitative Analysis software (B.07.00). MRM peaks of each modified nucleoside were extracted and normalized to the quantity of purified tRNA for each sample.

#### Live-cell imaging

For live-cell imaging of fluorescent fusion proteins, 3- to 4-week-old detached rice leaf sheaths of the susceptible cultivar CO-39 were inoculated with  $1 \times 10^5$  spores per ml of the indicated strains, unless otherwise stated. For each strain, time points and treatments were conducted using leaf sheaths from at least three different plants. Appressoria formation rates were calculated at 24 hpi from 50 germinating spores per strain, repeated in triplicate. Appressorial penetration rates were calculated at 30 hpi by determining how many of 50 appressoria per biological replicate, repeated in triplicate, had formed IH in rice cells by 30 hpi. Rates of spread of IH of the indicated strains to neighbouring cells by 48 hpi was calculated from 50 primary infected rice leaf sheath epidermal cells per biological replicate, repeated in triplicate. Infected detached rice leaf sheaths were imaged using a Nikon Eclipse Ni-E upright microscope and NIS Elements software. Excitation/emission was 488 nm/505-531 nm for GFP and 543 nm/590-632 nm for mCherry. For treatments, 1 mg ml<sup>-1</sup> paromomycin (Sigma-Aldrich) in 0.2% gelatin was added to cells at 36 hpi and its effects observed at 44 hpi. For the BFA assay, 4-week-old rice sheaths were inoculated with  $3 \times 10^4$  conidia per ml of each strain and incubated at 25 °C in the dark. At 36 hpi, the infected leaf sheath samples were infused with mock (0.1% DMSO in  $H_2O$ ) or freshly prepared BFA (50  $\mu$ g ml<sup>-1</sup> in 0.1% DMSO in  $H_2O$ ) at room temperature (23 °C), left for 4 h, then trimmed into ultrathin sections for imaging using Nikon Eclipse Ni-E Upright Microscope or, for best results, were further immersed in BFA and incubated at 23 °C for an additional 3 h.

#### **Vector construction**

The primers used for constructing the *UBA4-GFP* and *URM1-GFP* complementation vectors are in Supplementary Table 3. Briefly, *UBA4* and

*URM1* were amplified with the indicated primers to produce PCR products with 15–20 bases homologous to the pGTN vector. Purified PCR product was fused with linearized pGTN using the In-Fusion HD Cloning Kit (Clontech). The ligation mix was transferred into the *Escherichia coli* DH5a strain with ampicillin antibiotic screening, and all colonies were identified by PCR. Plasmids were sequenced to confirm they were error-free, then transformed into *M. oryzae* strains. *M. oryzae* transformants were screened by geneticin resistance and confirmed by PCR.

All other new vectors used in this study were constructed at Gen-Script USA, using the vector pBV591 as template. For the domain swap studies, BAS4 and its native promoter replaced PWL2 on pBV591 to give BAS4-mCherry:NLS; PWL2 and its native promoter replaced BAS4 to give PWL2-GFP. The PWL2 sequence and its native promoter were replaced in pBV591 by AVR-Pita or AVR-PIK and their native promoters to generate AVR-Pita-mCherry:NLS and AVR-Pik-mCherry:NLS (along with BAS4-GFP). The BAS4 sequence and native promoter were replaced in pBV591 with the SLP1 gene and its native promoter<sup>28</sup> to generate SLP1-GFP. For vectors carrying codon recoded genes, first, the recoded PWL2 (-AA $\rightarrow$  -AG) sequence replaced PWL2 in pBV591. Then, BAS4 in this  $PWL2(-AA \rightarrow -AG)$ -carrying vector was replaced with recoded Bas4 $(-AG \rightarrow -AA)$ . The PWL2, BAS4, PWL2(-AA $\rightarrow$ -AG), Bas4(-AG $\rightarrow$ -AA), AVR-Pita, AVR-Pik and SLP1 genes were synthesized at GenScript USA, subcloned onto the respective vectors using their Clone EZ method and confirmed by sequencing.

#### **qPCR**

Leaf sheath samples were collected at 42 hpi, and total RNA was extracted from each sample using the RNeasy mini kit (Qiagen). RNA was treated with DNase I (Invitrogen) and converted to cDNA using qScript (Quantas). qPCR was performed on a QuantStudio 3 real-time qPCR system (ThermoFischer Scientific) using the recommended reagents with primers listed in Supplementary Table 3. Thermocycler conditions were: 5 min at 95 °C, followed by 40 cycles of 95 °C for 30 s, 63 °C for 30 s and 68 °C for 1 min. qPCR data were analysed using the QuantStudio Design and Analysis software package (version 1.5.2), and fold changes were calculated using the  $\Delta\Delta$ Ct method  $^{51}$ .

#### Codon usage analysis

The complete coding sequence database of *M. oryzae*, which contains 12,836 protein coding sequences, was obtained from the Joint Genome Institute Genome portal (https://genome.jgi.doe.gov/portal/pages/dynamicOrganismDownload.jsf?organism=Magor1, project name: *Pyricularia oryzae* 70-15 v3.0). The codon usage pattern was analysed with CUSP, a command line program from EMBOSS (The European Molecular Biology Open Software Suite; http://bioinfo.pbi.nrc.ca:8090/EMBOSS/) (version 6.6), utilizing the high-performance computing resources provided by the Holland Computing Center at the University of Nebraska-Lincoln.

#### Statistics and reproducibility

Values represent the mean  $\pm$  s.d. of three independent biological replicates. Sample sizes were chosen based on previous studies in the field 22,25,27. Microsoft Excel 2016 was used to calculate the means  $\pm$  s.d. for the fluorescent protein distribution patterns during live-cell imaging. For comparing the mean values of the colony diameters, appressorium formation rates, penetration rates, cell-to-cell movement rates and lesion area rates, the one-way analysis of variance (ANOVA) function in PASW Statistics 18.0 (PASW Statistics) with the Tukey's honestly significant difference (HSD) multiple comparison test was used. For comparing the mean values of sporulation rates, the Welch ANOVA with Games–Howell post hoc test was used. For comparing the mean values of lesion areas, statistical analysis was performed with two-tailed unpaired t-test or one-way ANOVA with Tukey's multiple comparisons test, as indicated. For comparing target gene expression levels between different strains, the quantified transcript abundance

was calculated as the fold change as described in the figure legends, and statistical analysis was carried out using one-way ANOVA with the Student–Newman–Keuls test or the Tukey HSD multiple comparison tests in PASW Statistics. The R package agricolae was utilized to acquire precise *P* values for the Student–Newman–Keuls test, with modifications made to the source code of the SNK test function. A resulting *P* value of <0.05 was considered significant between group means.

#### **Reporting summary**

Further information on research design is available in the Nature Portfolio Reporting Summary linked to this article.

#### **Data availability**

The *M. oryzae UBA4* and *URM1* gene sequences are available at the National Center for Biotechnology Information (https://www.ncbi.nlm. nih.gov) under the accession numbers MGG\_05569 and MGG\_03978, respectively. Other gene sequences used in the course of this study can be found at the National Center for Biotechnology Information under the following accession numbers: MGG\_13863 for *PWL2*, MGG\_10914 for *BAS4*, MGG\_15370 for *AVR-Pita*, MGG\_10097 for *SLP1*, FJ807764 for *BAS1*, MGG\_18041 for *AvrPiz-t*, MGG\_10020 for *BAS107*, MGG\_05785 for *BAS113*, JN035619.1 for *AVR-Pik*, AB434708 for *Avr-Pia*, AF463528.1 for *AVR1-CO39*, and AAK31287.1 for *TOXB*. Strains generated during the course of this study are available from the corresponding author upon request and with an appropriate Animal and Plant Health Inspection Service permit. Source data are provided with this paper.

#### **Code availability**

Underlying source code associated with the P value calculations in Fig. 4e is available in Source Data Fig. 4.

#### References

- Björk, G. R., Huang, B., Persson, O. P. & Byström, A. S. A conserved modified wobble nucleoside (mcm<sup>5</sup>s<sup>2</sup>U) in lysyl-tRNA is required for viability in yeast. RNA 13, 1245–1255 (2007).
- Dewez, M. et al. The conserved wobble uridine tRNA thiolase Ctu1-Ctu2 is required to maintain genome integrity. Proc. Natl Acad. Sci. USA 105, 5459–5464 (2008).
- Rezgui, V. A. et al. tRNA t<sup>KUUU</sup>, tQ<sup>UUG</sup>, and tE<sup>UUC</sup> wobble position modifications fine-tune protein translation by promoting ribosome A-site binding. *Proc. Natl Acad. Sci. USA* 110, 12289–12294 (2013).
- Zinshteyn, B. & Gilbert, W. V. Loss of a conserved tRNA anticodon modification perturbs cellular signaling. *PLoS Genet.* 9, e1003675 (2013).
- Boccaletto, P. et al. MODOMICS: a database of RNA modification pathways. Nucleic Acids Res. 46, D303–D307 (2018).
- Laxman, S. et al. Sulfur amino acids regulate translational capacity and metabolic homeostasis through modulation of tRNA thiolation. Cell 154, 416–429 (2013).
- Nedialkova, D. D. & Leidel, S. A. Optimization of codon translation rates via tRNA modifications maintains proteome integrity. *Cell* 161, 1606–1618 (2015).
- Chou, H. J. et al. Transcriptome-wide analysis of roles for tRNA modifications in translational regulation. *Mol. Cell* 68, 978–992 (2017).
- Gupta, R. et al. A tRNA modification balances carbon and nitrogen metabolism by regulating phosphate homeostasis. *eLife* 8, e44795 (2019).
- Dean, R. A. et al. The genome sequence of the rice blast fungus Magnaporthe grisea. Nature 434, 980–986 (2005).
- Wilson, R. A. & Talbot, N. J. Under pressure: investigating the biology of plant infection by *Magnaporthe oryzae*. *Nat. Rev. Microbiol.* 7, 185–195 (2009).

- Fernandez, J. & Orth, K. Rise of a cereal killer: the biology of Magnaporthe oryzae biotrophic growth. Trends Microbiol. 26, 582–597 (2018).
- 13. Cruz-Mireles, N., Eseola, A. B., Osés-Ruiz, M., Ryder, L. S. & Talbot, N. J. From appressorium to transpressorium—defining the morphogenetic basis of host cell invasion by the rice blast fungus. *PLoS Pathog.* **17**, e1009779 (2021).
- Wilson, R. A. Magnaporthe oryzae. Trends Microbiol. 29, 663–664 (2021).
- Pabis, M. et al. Molecular basis for the bifunctional Uba4– Urm1 sulfur-relay system in tRNA thiolation and ubiquitin-like conjugation. EMBO J. 39, e105087 (2020).
- Leidel, S. et al. Ubiquitin-related modifier Urm1 acts as a sulphur carrier in thiolation of eukaryotic transfer RNA. *Nature* 458, 228–232 (2009).
- Rapino, F. et al. Wobble tRNA modification and hydrophilic amino acid patterns dictate protein fate. Nat. Commun. 12, 2170 (2021).
- Shigi, N. Recent advances in our understanding of the biosynthesis of sulfur modifications in tRNAs. Front. Microbiol. 9, 2679 (2018).
- Wilson, R. A., Gibson, R. P., Quispe, C. F., Littlechild, J. A. & Talbot, N. J. An NADPH-dependent genetic switch regulates plant infection by the rice blast fungus. *Proc. Natl Acad. Sci. USA* 107, 21902–21907 (2010).
- Valent, B., Farrall, L. & Chumley, F. G. Magnaporthe grisea genes for pathogenicity and virulence identified through a series of backcrosses. Genetics 127, 87–101 (1991).
- Ryder, L. S. et al. A sensor kinase controls turgor-driven plant infection by the rice blast fungus. Nature 574, 423–427 (2019).
- Rocha, R. O., Elowsky, C., Pham, N. T. T. & Wilson, R. A. Spermine-mediated tight sealing of the Magnaporthe oryzae appressorial pore-rice leaf surface interface. Nat. Microbiol. 5, 1472–1480 (2020).
- 23. Kankanala, P., Czymmek, K. & Valent, B. Roles for rice membrane dynamics and plasmodesmata during biotrophic invasion by the blast fungus. *Plant Cell* **19**, 706–724 (2007).
- 24. Giraldo, M. C. et al. Two distinct secretion systems facilitate tissue invasion by the rice blast fungus *Magnaporthe oryzae*. *Nat. Commun.* **4**, 1996 (2013).
- Sun, G., Elowsky, C., Li, G. & Wilson, R. A. TOR-autophagy branch signaling via Imp1 dictates plant-microbe biotrophic interface longevity. *PLoS Genet.* 14, e1007814 (2018).
- Khang, C. H. et al. Translocation of Magnaporthe oryzae effectors into rice cells and their subsequent cell-to-cell movement. Plant Cell 22, 1388–1403 (2010).
- Marroquin-Guzman, M. et al. The Magnaporthe oryzae nitrooxidative stress response suppresses rice innate immunity during blast disease. Nat. Microbiol. 2, 17054 (2017).
- 28. Mentlak, T. A. et al. Effector-mediated suppression of chitin-triggered immunity by *Magnaporthe oryzae* is necessary for rice blast disease. *Plant Cell* **24**, 322–335 (2012).
- Rabouille, C. Pathways of unconventional protein secretion. Trends Cell Biol. 27, 230–240 (2017).
- Park, C. H. et al. The Magnaporthe oryzae effector AvrPiz-t targets the RING E3 ubiquitin ligase APIP6 to suppress pathogen-associated molecular pattern-triggered immunity in rice. Plant Cell 24, 4748–4762 (2012).
- de Guillen, K. et al. Structure analysis uncovers a highly diverse but structurally conserved effector family in phytopathogenic fungi. PLoS Pathog. 11, e1005228 (2015).
- Sperschneider, J., Dodds, P. N., Singh, K. B. & Taylor, J. M. ApoplastP: prediction of effectors and plant proteins in the apoplast using machine learning. *New Phytol.* 217, 1764–1778 (2018).

- 33. Yan, X. et al. The transcriptional landscape of plant infection by the rice blast fungus *Magnaporthe oryzae* reveals distinct families of temporally co-regulated and structurally conserved effectors. *Plant Cell* **35**, 1360–1385 (2023).
- Yoshida, K. et al. Association genetics reveals three novel avirulence genes from the rice blast fungal pathogen Magnaporthe oryzae. Plant Cell 21, 1573–1591 (2009).
- 35. Ribot, C. et al. The *Magnaporthe oryzae* effector AVR1-CO39 is translocated into rice cells independently of a fungal-derived machinery. *Plant J.* **74**, 1–12 (2013).
- Stuart, L. M., Paquette, N. & Boyer, L. Effector-triggered versus pattern-triggered immunity: how animals sense pathogens. *Nat. Rev. Immunol.* 13, 199–206 (2013).
- 37. Liu, T. et al. Unconventionally secreted effectors of two filamentous pathogens target plant salicylate biosynthesis. *Nat. Commun.* **5**, 4686 (2014).
- 38. Balmer, E. A. & Faso, C. The road less traveled? Unconventional protein secretion at parasite–host interfaces. *Front. Cell Dev. Biol.* **9**, 662711 (2021).
- Rapino, F. et al. Codon-specific translation reprogramming promotes resistance to targeted therapy. *Nature* 558, 605–609 (2018).
- Pechmann, S., Chartron, J. W. & Frydman, J. Local slowdown of translation by nonoptimal codons promotes nascent-chain recognition by SRP in vivo. Nat. Struct. Mol. Biol. 21, 1100–1105 (2014).
- Stuer, N., Van Damme, P., Goormachtig, S. & Van Dingenen, J. Seeking the interspecies crosswalk for filamentous microbe effectors. *Trends Plant Sci.* https://doi.org/10.1016/j.tplants. 2023.03.017 (2023).
- 42. Ikeuchi, K. et al. Collided ribosomes form a unique structural interface to induce Hel2-driven quality control pathways. *EMBO J.* **38**, e100276 (2019).
- Juszkiewicz, S. et al. Ribosome collisions trigger cis-acting feedback inhibition of translation initiation. *eLife* 9, e60038 (2020).
- 44. Weber, R. et al. 4EHP and GIGYF1/2 mediate translation-coupled messenger RNA decay. *Cell Rep.* **33**, 108262 (2020).
- Doma, M. K. & Parker, R. Endonucleolytic cleavage of eukaryotic mRNAs with stalls in translation elongation. *Nature* 440, 561–564 (2006).
- D'Orazio, K. N. et al. The endonuclease Cue2 cleaves mRNAs at stalled ribosomes during No Go Decay. eLife 8, e49117 (2019).
- Navickas, A. et al. No-Go Decay mRNA cleavage in the ribosome exit tunnel produces 5'-OH ends phosphorylated by Trl1. Nat. Commun. 11, 122 (2020).
- Liu, Y. A code within the genetic code: codon usage regulates co-translational protein folding. Cell Commun. Signal. 18, 145 (2020).
- 49. Yan, M. et al. A high-throughput quantitative approach reveals more small RNA modifications in mouse liver and their correlation with diabetes. *Anal. Chem.* **85**, 12173–12181 (2013).
- 50. Su, D. et al. Quantitative analysis of ribonucleoside modifications in tRNA by HPLC-coupled mass spectrometry. *Nat. Protoc.* **9**, 828–841 (2014).
- Livak, K. J. & Schmittgen, T. D. Analysis of relative gene expression data using real-time quantitative PCR and the 2<sup>-ΔΔCT</sup> method. Methods 25, 402–408 (2001).

#### **Acknowledgements**

This work was supported by the National Science Foundation (IOS-1758805 and IOS-2106153). Z.G. was supported by funding from the China Scholarship Council (file number 201903250119). Bioinformatic analyses were completed using the supercomputing

resources of the Holland Computing Center at the University of Nebraska-Lincoln, which receives support from the Nebraska Research Initiative.

#### **Author contributions**

R.A.W. conceived the project and obtained funding. R.A.W. designed the experiments. R.A.W. and G.L. interpreted the data. G.L., N.D. and Z.G. generated the strains and performed the experiments. G.L. performed the bioinformatic analyses. R.A.W. wrote the paper, with contributions from all authors.

#### **Competing interests**

The authors declare no competing interests.

#### **Additional information**

**Extended data** is available for this paper at https://doi.org/10.1038/s41564-023-01443-6.

**Supplementary information** The online version contains supplementary material available at https://doi.org/10.1038/s41564-023-01443-6.

**Correspondence and requests for materials** should be addressed to Richard A. Wilson.

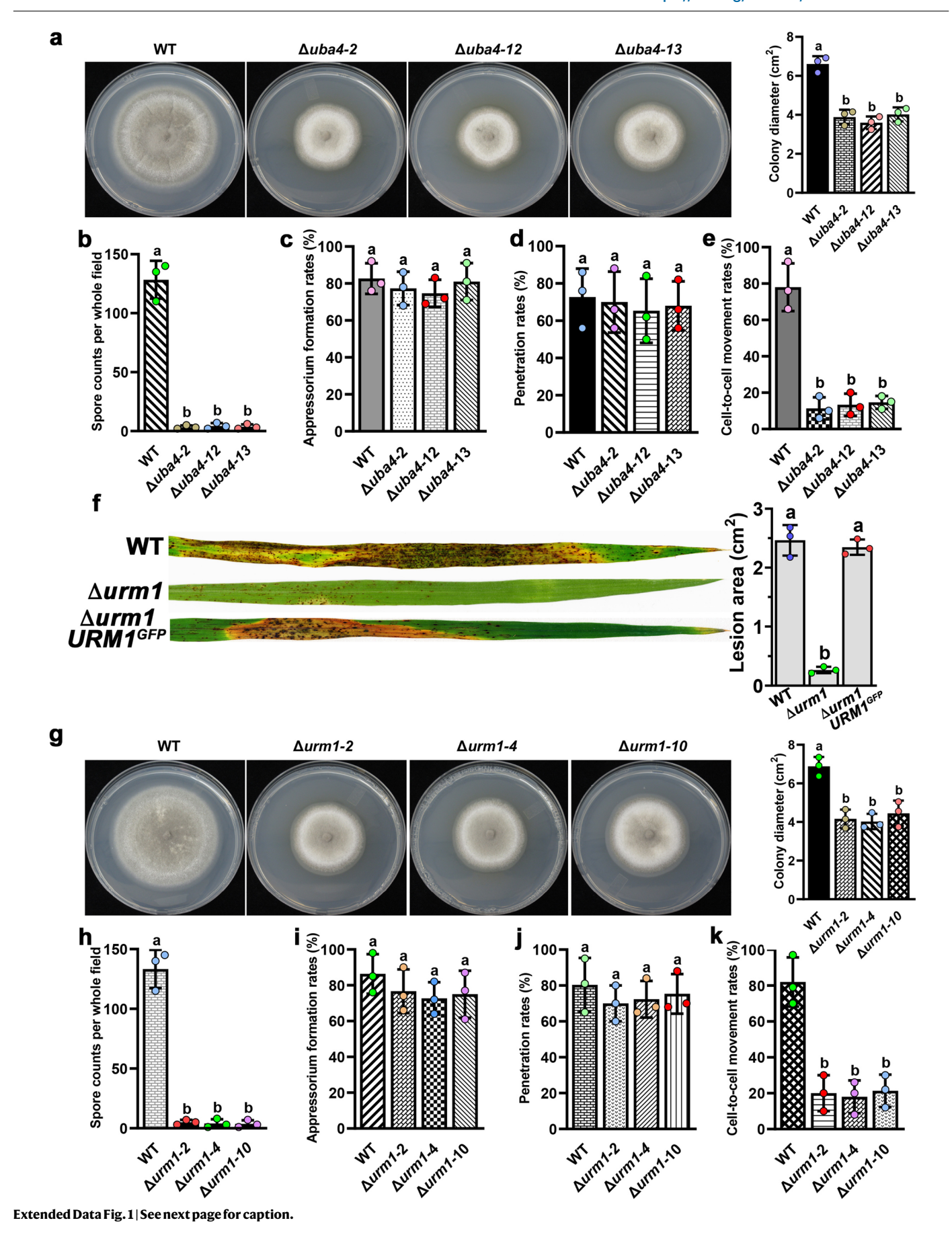
**Peer review information** *Nature Microbiology* thanks the anonymous reviewers for their contribution to the peer review of this work. Peer reviewer reports are available.

**Reprints and permissions information** is available at www.nature.com/reprints.

**Publisher's note** Springer Nature remains neutral with regard to jurisdictional claims in published maps and institutional affiliations.

Springer Nature or its licensor (e.g. a society or other partner) holds exclusive rights to this article under a publishing agreement with the author(s) or other rightsholder(s); author self-archiving of the accepted manuscript version of this article is solely governed by the terms of such publishing agreement and applicable law.

© The Author(s), under exclusive licence to Springer Nature Limited 2023



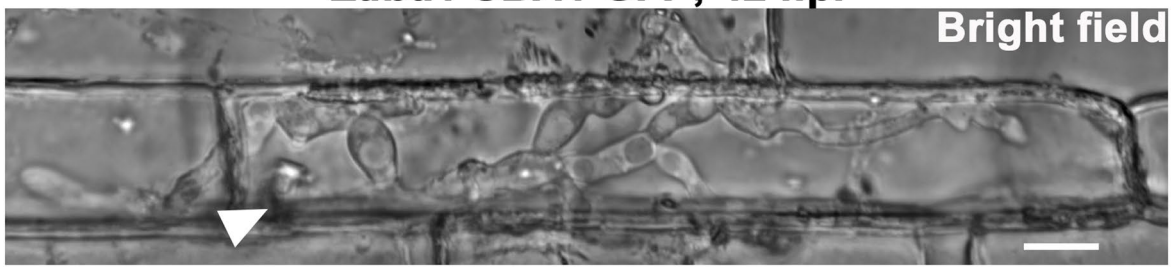
Extended Data Fig. 1 | Loss of *UBA4* or *URM1* in *M. oryzae* impairs biotrophic growth in host rice cells. a-e, Three independent transformants carrying deletions in *UBA4* had identical phenotypes. Compared to WT,  $\Delta uba4$  strains were reduced in radial growth (a) and sporulation (b) on complete media (CM) by 10 days post inoculation (dpi), but appressorium formation rates on detached rice leaf sheath surfaces at 24 hpi (c), and penetration rates of appressoria on host rice leaf sheath surfaces at 30 hpi (d), were not affected by the loss of *UBA4*; however, cell-to-cell movement of  $\Delta uba4$  invasive hyphae (IH) from the first infected rice cell into neighbouring cells at 48 hpi was reduced (e). f, Compared to WT and the  $\Delta urm1 URM1$ -GFP complementation strain, loss of *URM1* abolished *M. oryzae* pathogenicity on rice leaves. *Left*, Leaves were imaged at 5 dpi. Images are representative of at least 5 leaves from three biological replicates. *Right*, 10 cm lengths of infected rice leaves were imaged at 5 dpi. Disease lesion areas were quantified using Image I and analyzed according to one-way ANOVA

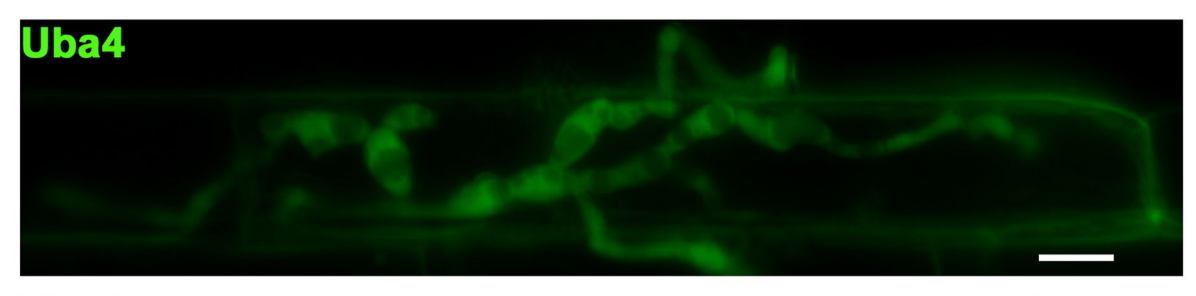
followed by a Tukey HSD test for multiple comparisons. Values are the means  $\pm$  s.d. from three biological replicates. Different letters indicate significant differences (p < 0.05). **g-k**, Three independent transformants carrying deletions in *URM1* had identical phenotypes, and also strongly resembled the  $\Delta uba4$  strains in growth (**g**), sporulation rates (**h**), appressorium formation (**i**) and function (**j**), and cell-to-cell movement rates (**k**), compared to WT. **a,g**, Colonies of each strain were imaged and measured after 10 days growth on CM. Images are representative of three independent experiments. **a-e**, **g-k**, Values are means  $\pm$  s.d. from three biological replicates. Bars with different letters indicate significant differences at  $P \le 0.05$ . P-values were determined by one-way ANOVA with Tukey's multiple comparisons test (**a**, **c-g**, **i-k**) or by Welch ANOVA with Games-Howell post hoc test (**b**, **h**). Exact P values are given in **Source Data Extended Data Fig. 1. c, i**, Spores of the indicated strains were inoculated onto detached rice leaf sheaths at a rate of  $0.5 \times 10^5$  spores ml<sup>-1</sup>.

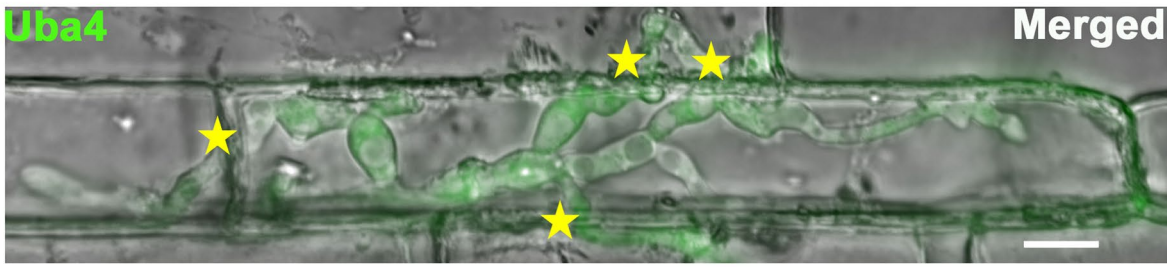
Uba4

Werged





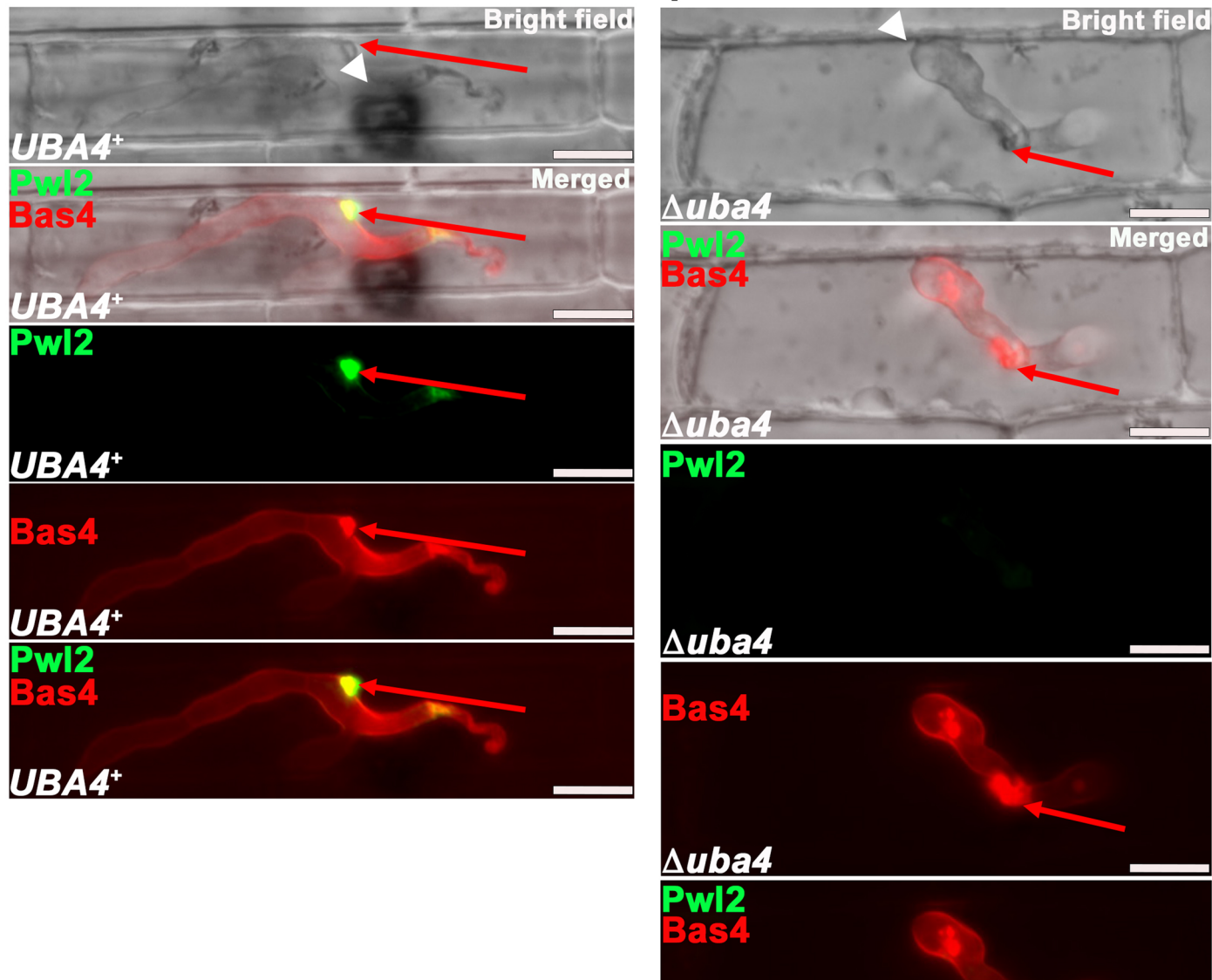




Extended Data Fig. 2 | Uba4 is localized to the cytoplasm in invasive hyphae. Live-cell imaging of the  $\Delta uba4$  UBA4-GFP complementation strain in detached rice leaf sheath epidermal cells at 38 hpi and 42 hpi shows that the Uba4-GFP fusion protein localizes to the cytoplasm of fungal invasive hyphae. White

arrowheads indicate penetration sites, stars indicate movement of invasive hyphae into neighbouring cells. Scale bars, 10  $\mu m$ . Representative images are based on the observations of 50 infected rice cells per leaf sheath per treatment, repeated in triplicate.

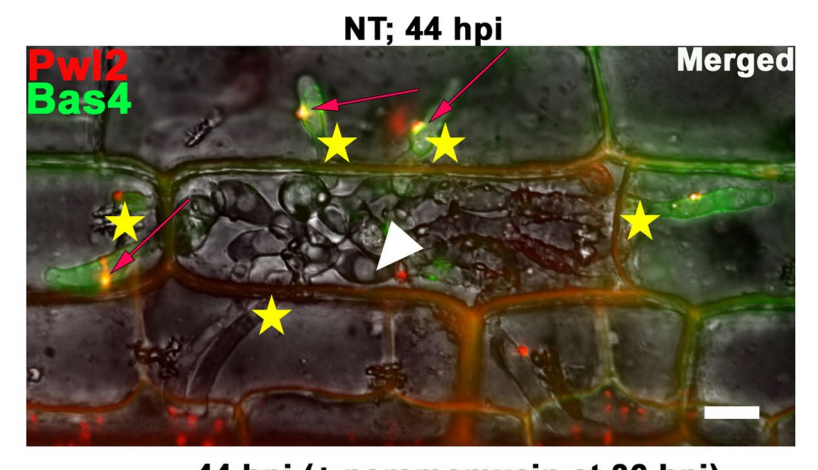
# 36 hpi

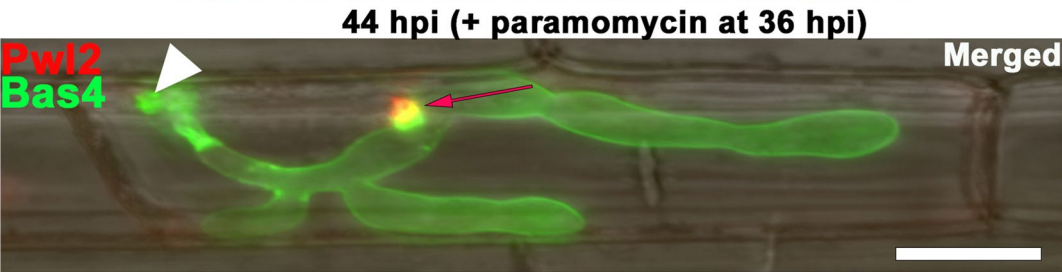


Extended Data Fig. 3 | Bas4-mCherry:NLS but not Pwl2-GFP is secreted by  $\Delta uba4$ . Live-cell imaging at 36 hpi of the indicated strains expressing PWL2-GFP and BAS4-mCherry:NLS in detached rice leaf sheath epidermal cells shows how in 100 % of observed infected cells, Pwl2-GFP accumulated in BICs of the  $UBA4^*$  strain but not in  $\Delta uba4$  BICs, while Bas4-mCherry:NLS accumulated in the

apoplast of both strains. Calculations and representative images are based on the observations of 50 infected rice cells per leaf sheath per treatment, repeated in triplicate. White arrowheads indicate penetration sites; red arrows indicate Pwl2 in BICs. Scale bars, 10  $\mu m$ .

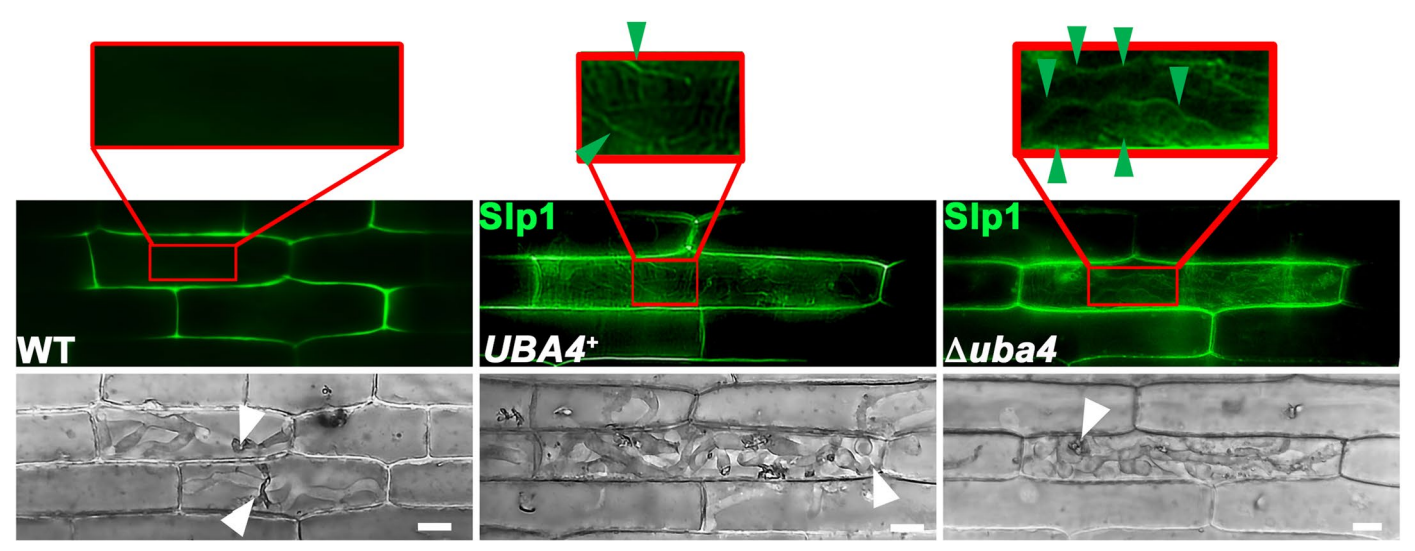
∆uba4





Extended Data Fig. 4 | Paromomycin treatment impairs biotrophic growth in WT but does not prevent effector translation or secretion. Live-cell imaging at 44 hpi of detached rice leaf sheath epidermal cells colonized with the wild type Guy11 strain expressing *PWL2-mCherry:NLS* and *BAS4-GFP*. Compared to the non-treated (NT) control (*Top*), treatment with paromomycin at 36 hpi (*Bottom*) impaired biotrophic growth and prevented cell-to-cell spread of invasive hyphae

by 44 hpi, but effectors were nonetheless translated and secreted, and the BIC and apoplastic space were intact. White arrowheads indicate penetration sites; red arrows indicate Pwl2 in BICs; stars indicate movement of invasive hyphae into neighbouring cells. Scale bars, 10  $\mu m$ . Representative images are based on the observations of 50 infected rice cells per leaf sheath per treatment, repeated in triplicate.



**Extended Data Fig. 5** | **Slp1 is secreted into the**  $\Delta uba4$  **apoplast.** Live-cell imaging at 44 hpi of detached rice leaf sheath epidermal cells infected with the indicated strains expressing *SLP1*-GFP shows how in 100 % of observed infected cells, compared to WT lacking *SLP1*-GFP, Slp1 accumulated in the apoplast of both  $UBA4^+$  and  $\Delta uba4$  strains. Slp1-GFP fluorescence was weak in both strains and

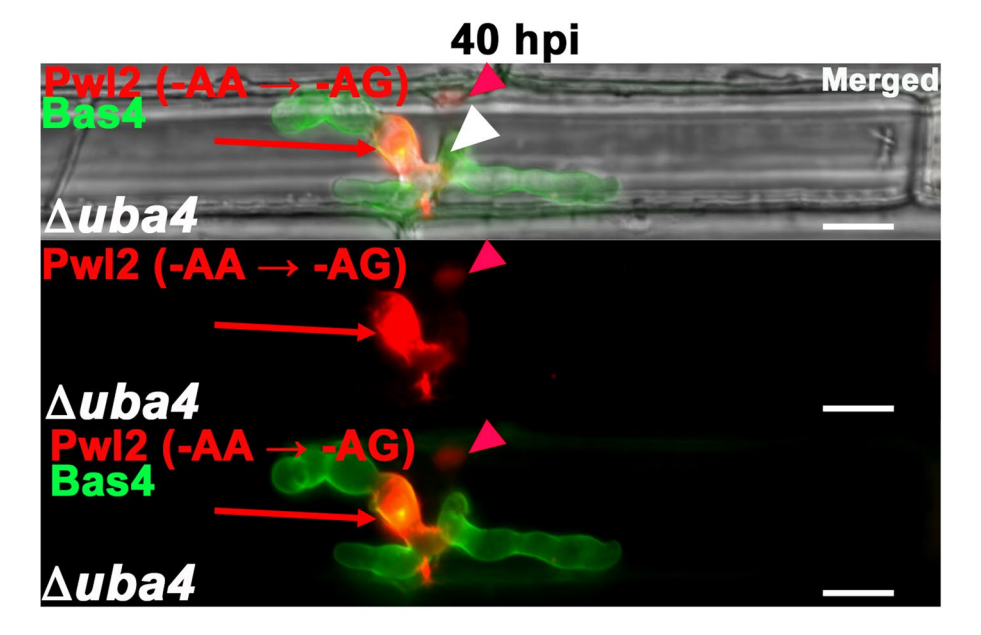
can be best seen outlining IH in the blow-up boxes, indicated with green arrow heads. Calculations and representative images are based on the observations of 50 infected rice cells per leaf sheath per treatment, repeated in triplicate. White arrowheads indicate penetration sites. Scale bars,  $10~\mu m$ .

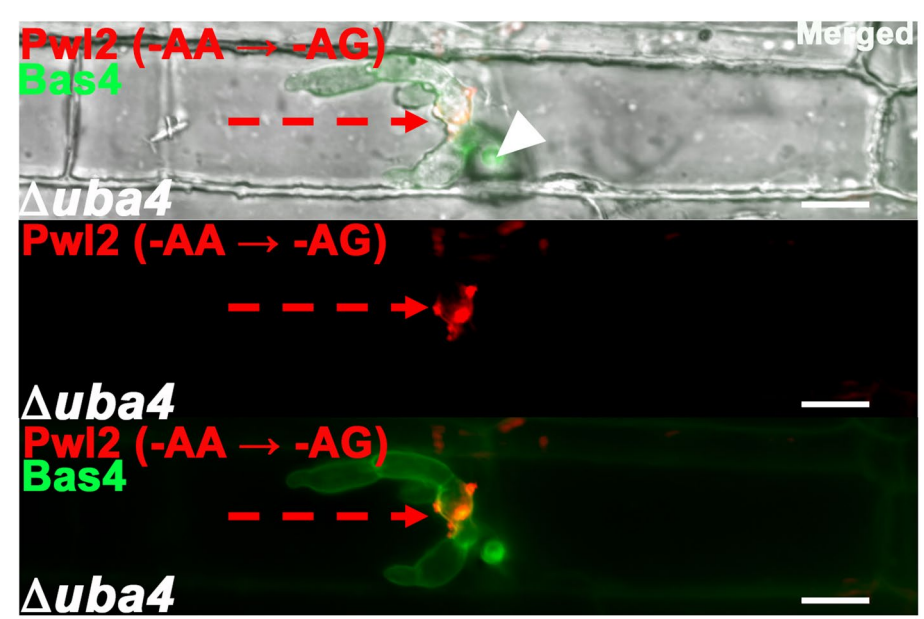
#### Pwl2-mCherry: NLS

```
AAA (Lys) to AAG (Lys) (7)
CAA (Gln) to CAG (Gln) (3)
GAA (Glu) to GAG (Glu) (9)
```

atg aaa tgc aac atc atc ctc cct ttt gct ttg gtc ttt ttt tcg acc act gta acc Р K C Ν Ι Ι L F Α L V F F S Τ Т Τ tgg act aac aaa caa ttt tac aac qcc ggt ggc ggg gac aaa ggc gaa aga gag qqc tca Т Α G G G W Ν K Q F Υ Ν D K G Ε R Ε G S att gaa ggc tca att ttt aac tat ggc ccc agt tat cct agg aaq ggc tcg gat gga ggg Ι R K G S Ε G D F Ν Y G Р S Y G G atg gat agg gta cgg gtt cat **gaa** aac ggc aac atc CCC CCC atq aac cqc ggg ccq gga VV Ε R Ρ Р Ρ D R Μ R H Ν Ν G Ν Ι G M G tct cta ggc tat cct gat cat caq gaa gat aaa agc gat cgt caa tat tat aac agg cac S  $\mathbf{L}$ G Р D Η Q Ε D K S D R Q. Υ Y Ν R Η gga tat cat gtt ggt gat qqa CCC qcc gaa tac gga aat cac gga aac ggg taa aac Y Η V D G Ρ Α Ε Y G Ν Η G G W G G G 0 G gac gga tat tat gga ccg cca ggc gag ttt aca cat gag cac cgt gaa cag cga gaa gag Ρ Р G Ε F Т D G Y Υ G Η Ε Η R Ε Q R Ε Ε gtg att atq tcc atq aaq atq atc atc tgc aat gga agc ggc gag gag gat aac qcc K Ε G C Ν Ι Μ G S М V S G  $\mathbf{E}$ D Ν М Α Ι Ι atq cqc ttc qtq cac atq gag tcc qtq aaq gag ttc aaq ggc aac ggc cac gag ttc gag K F М R F K V Η Ε V Ν Η Ε F Ε Ε M G S G cag gcc aag ctg aag atc gag ggc gag ggc gag ggc cgc ccc tac gag ggc acc acc ata Ι Ε G G Ε G R Ρ Υ Ε G Т Q Τ Α K L K V ccc ctg CCC ttc gcc gac atc ctg tcc cct cag ttc acc aag ggt ggc tgg atg tac ggc Τ K G Р L Р F Α W D Ι  $\mathbf{L}$ S Р Q F М Y G G tcc ttc tcc aag gcc tac gtg aag cac ccc gcc gac atc ccc gac tac ttg aag ctq CCC Р Р Р S K A Υ 77 K Η Α D Ι D Y  $\mathbf{L}$ K  $\mathbf{L}$ S gag ggc ttc aag tgg gag cgc gtg atg aac ttc gag gac ggc ggc gtg gtg acc gtg Ε G F K W Ε R V М Ν F Ē D G G V V Τ V Т gac gtg ggc acc cag gac tcc tcc ctg cag ggc gag ttc atc tac aaq aaq ctq cgc aac F Т S S  $\mathbf{L}$ Q D G Ε Ι Υ K V K  $\mathbf{L}$ R G Ν ttc CCC tcc gac ggc ccc qta atq caq aaq aaq acc atq tcc tcc aac taa gag qcc gag Ρ Τ S D G V М Q K K Μ G Ε Α Ε qcc ctg aaq atc ctq cqq atq tac CCC gag gac ggc ggc gag aag cag agg aag ctg aag R Y Р Ε D G Α  $\mathbb{L}$ K G Ε Ι K R L K L K М Q acc acc gcc aag cag ggc ggc cac tac gac gct gag gtc aag tac aag aag CCC gtg gac Τ Τ  $\bigvee$ D G G Η Y D Α Ε V K Y K Α K K Ρ Q ctg ccc ggc gcc tac aac gtc aac atc ttg gac atc acc cac aac aag tcc gag gac tac T. P G Α Y Ν V Ν Ι K  $\mathbf{L}$ D Ι Т S Η Ν Ε D Y cac tcc acc atc ata gaa caq tac gaa cac acc gag ggc cac acc ggc aac atq gag gag Y Τ Τ V Ε R A Ε G R Η S G М Ε  $\mathbf{E}$ Ι  $\mathbf{E}$ Q G tac aag gat ctq gga ctc aga tct cga gct gat cca aag aag aga aag cca gta K R R Р K K K R K V Р  $\mathbf{L}$ Υ G L S Α D  $\square$ aaa aaq aag aga aaq gta gat cca aaa aag aag aga aag gta gga tct taa K V D Р K K K R K V G S

**Extended Data Fig. 6** | **Location of AA-ending codons in** *PWL2-mCherry:NLS*. AA-ending codons in the *PWL2-mCherry:NLS* coding sequence  $^{26}$  that were recoded to synonymous AG-ending codons in *PWL2* ( $-AA \rightarrow -AG$ ) are shown in red. The first *mCherry* codon is highlighted in yellow. The start of the *NLS* sequence is highlighted in green. The linker sequence is highlighted in grey.



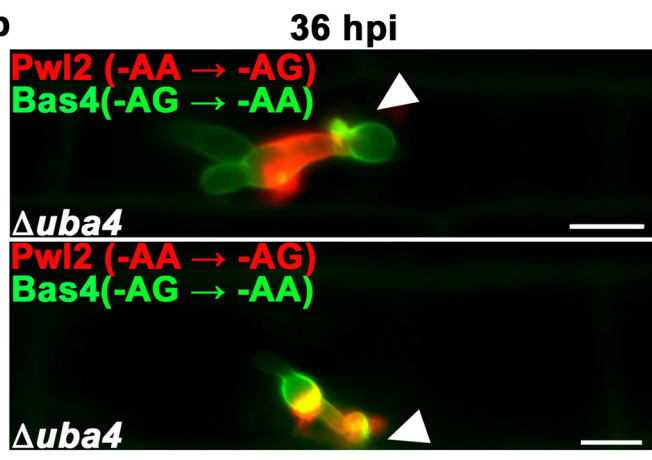


**Extended Data Fig. 7** | **Expressing** *PWL2 (-AA*  $\rightarrow$  *-AG)* in  $\triangle$  *uba4* affects BIC **integrity.** Live-cell imaging at 40 hpi of detached rice leaf sheath epidermal cells infected with  $\triangle$  *uba4* expressing *PWL2 (-AA*  $\rightarrow$  *-AG)* and *BAS4-GFP*. White arrowheads indicate penetration sites; red arrowheads indicate recoded Pwl2 in

host nuclei; solid red arrows indicate recoded Pwl2 in enlarged BICs; dashed red arrows indicate recoded Pwl2 in fractured BICs. Scale bars,  $10~\mu m$ . Representative images are based on the observations of 50 infected rice cells per leaf sheath per treatment, repeated in triplicate.

AAG (Lys) to AAA (Lys) (22)
CAG (Gln) to CAA (Gln) (10)
GAG (Glu) to GAA (Glu) (20)

atq caq ctc tca ttc tca gca atc gcc atc ctt ttg gcc ttc gcc gtc aac cac gct acg cga ctc tgc cat gat gcc gac gga ctt ggc gct gga tcc gtg agc aag ggc gag gag ctg ttc acc ggg aac ggc cac aag ttc agc gtg acc ctg acc tac aac ata ttc aag tcc gcc atg ccc tac aaσ acc cac aac atc cgc cac aac aac acc ccc atc ggc gac ttc gtg acc gcc gcc ggg atc act ctc ggc atg ctg tac aag taa Υ K



Extended Data Fig. 8 | See next page for caption.

**Extended Data Fig. 8** | **Expressing BAS4** ( $AG \rightarrow -AA$ ) in  $\Delta uba4$  does not affect **Bas4 secretion.** a, AG-ending codons in the BAS4-GFP coding sequence <sup>26</sup> that were recoded to synonymous AA-ending codons in BAS4 ( $-AG \rightarrow -AA$ ) are shown in red. The GFP start codon is highlighted in green. The linker sequence is highlighted in grey. **b**, Live-cell imaging at 36 hpi of detached rice leaf sheath

epidermal cells infected with  $\Delta uba4$  expressing PWL2 ( $AA \rightarrow AG$ ) and BAS4 ( $AG \rightarrow AG$ ). Recoded Bas4 and recoded Pwl2 are correctly deployed, albeit sometimes resulting in enlarged or fractured BICs in the latter case. White arrowheads indicate penetration sites. Scale bars, 10  $\mu$ m. Images are based on the observations of 50 infected rice cells per leaf sheath, repeated in triplicate.

a

	∑CDS			BAS4	
Codon	Fraction	Number	Codon	Fraction	Number
GAA	0.296	98391	GAA	0	0
GAG	0.704	234297	GAG	1	5
AAA	0.249	66217	AAA	0.4	2
AAG	0.751	199963	AAG	0.6	3
CAA	0.338	77501	CAA	0	0
CAG	0.662	151801	CAG	1	2
	PWL2		AVR-Pita		
Codon	Fraction	Number	Codon	Fraction	Number
GAA	0.64	7	GAA	0.86	12
GAG	0.36	4	GAG	0.14	2
AAA	8.0	4	AAA	0.92	12
AAG	0.2	1	AAG	0.08	1
CAA	0.6	3	CAA	0.83	5
CAG	0.4	2	CAG	0.17	1

SLP1					
Codon	Fraction	Number			
GAA	0	0			
GAG	0	0			
AAA	0	0			
AAG	1	5			
CAA	0.11	1			
CAG	0.89	8			

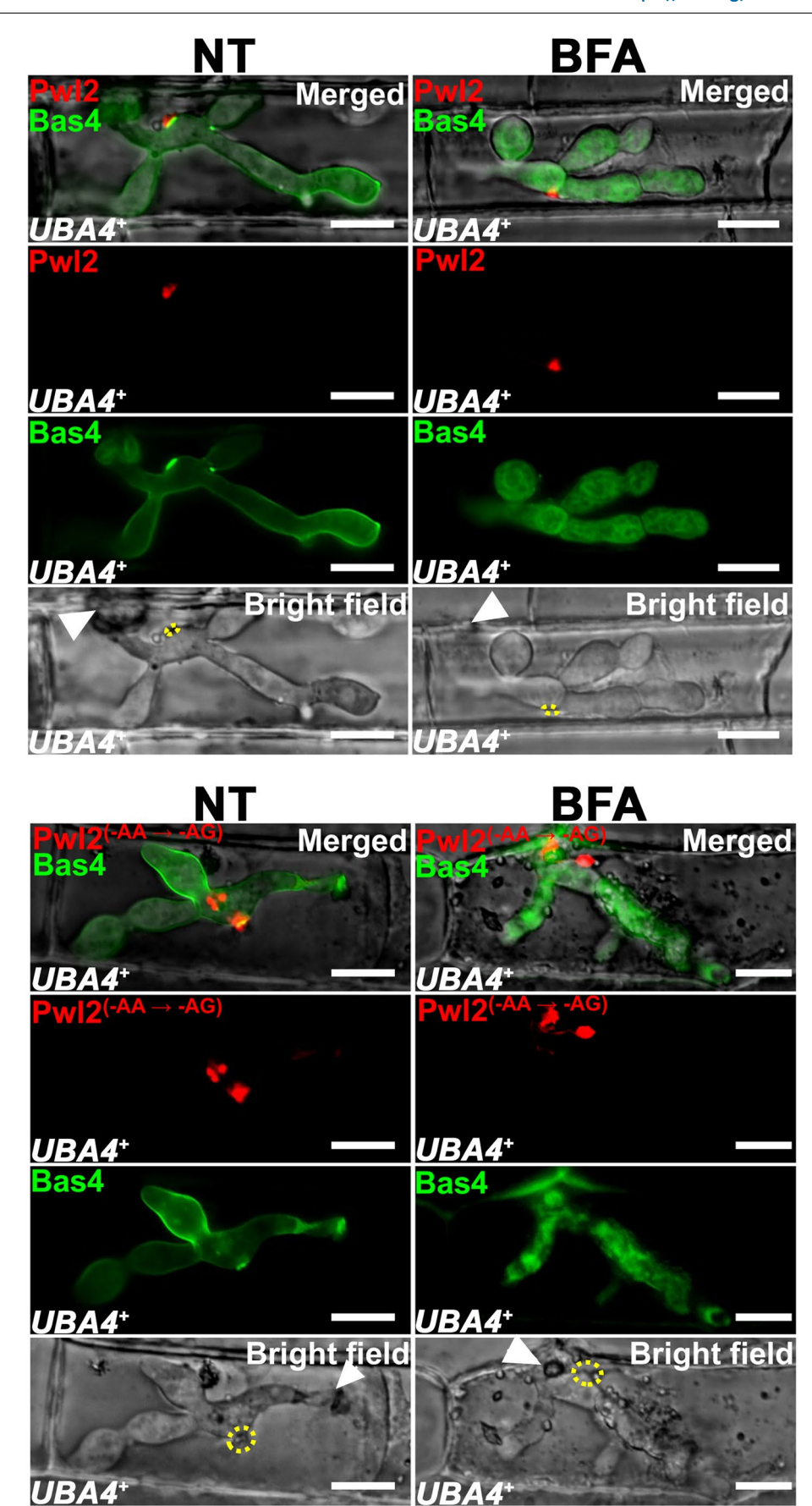
b

D								
		BAS1		AvrPiz-t				
	Codon	Fraction	Number	Codon	Fraction	Number		
	GAA	0.44	4	GAA	1	2		
	GAG	0.56	5	GAG	0	0		
	AAA	0.6	3	AAA	0.5	3		
	AAG	0.4	2	AAG	0.5	3		
	CAA	0.88	7	CAA	0.33	2		
	CAG	0.13	1	CAG	0.67	4		
	BAS107		BAS113					
	Codon	Fraction	Number	Codon	Fraction	Number		
	GAA	0.5	4	GAA	0.14	4		
	GAG	0.5	4	GAG	0.86	4		
	AAA	0.45	5	AAA	0.08	2		
	AAG	0.55	6	AAG	0.92	23		
	CAA	0.67	4	CAA	0.25	4		

C

	AVR-Pik			AVR-Pia			AVR1-CO3	9		TOXB	
Codon	Fraction	Number									
GAA	0.75	3	GAA	0.75	3	GAA	0.33	2	GAA	0.33	1
GAG	0.25	1	GAG	0.25	1	GAG	0.67	4	GAG	0.67	2
AAA	1	8	AAA	1	4	AAA	0	0	AAA	0	0
AAG	0	0	AAG	0	0	AAG	4	1	AAG	1	2
CAA	1	1	CAA	0.5	1	CAA	1	2	CAA	1	2
CAG	0	0	CAG	0.5	1	CAG	0	0	CAG	0	0

Extended Data Fig. 9 | AA- and AG-ending codon counts for apoplastic and cytoplasmic effector mRNAs. Tables showing frequencies and numbers of synonymous AA-ending (red) and AG-ending (black) codons in all M. oryzae protein coding sequences ( $\Sigma$ CDS) (a) and in the indicated effector-encoding mRNAs (a-c). See text for details.



Extended Data Fig. 10 | See next page for caption.

**Extended Data Fig. 10** | **Brefeldin A treatment did not affect the secretion of recoded Pwl2 into the BIC.** Live-cell imaging at 40 hpi of detached rice leaf sheath epidermal cells infected with  $UBA4^+$  strains expressing BAS4-GFP and either PWL2 (Top) or recoded PWL2 ( $AA \rightarrow -AG$ ) (Bottom) shows how in both cases, and in 100 % of observed cells, Brefeldin A (BFA) treatment, which inhibits conventional ER-Golgi secretion, led to the retention of Bas4 in IH cytoplasm as expected, but Pwl2 secretion into the BIC was unaffected. This confirms that recoded Pwl2 ( $-AA \rightarrow -AG$ ) is, like Pwl2, secreted into the BIC via

the unconventional protein secretion pathway and that, moreover, no spillover secretion of Pwl2 (-AA  $\rightarrow$  -AG) through the ER-Golgi pathway contributes to the enlarged, split-BIC phenotype observed for this strain. White arrowheads indicate penetration sites; hatched yellow circles indicate BICs, which are enlarged in the *UBA4*\* *PWL2* (-AA  $\rightarrow$  -AG) strain compared to the *UBA4*\* *PWL2* strain. Scale bars, 10  $\mu$ m. Calculations and representative images are based on the observations of 50 infected rice cells per leaf sheath per treatment, repeated in triplicate.

# nature portfolio

Corresponding author(s):	Richard A. Wilson
Last updated by author(s):	Jun 26, 2022

# **Reporting Summary**

Nature Portfolio wishes to improve the reproducibility of the work that we publish. This form provides structure for consistency and transparency in reporting. For further information on Nature Portfolio policies, see our <u>Editorial Policies</u> and the <u>Editorial Policy Checklist</u>.

_				
7	ta	ŤΙ	らた	ICS

For	all statistical analyses, confirm that the following items are present in the figure legend, table legend, main text, or Methods section.
n/a	Confirmed
	The exact sample size (n) for each experimental group/condition, given as a discrete number and unit of measurement
	A statement on whether measurements were taken from distinct samples or whether the same sample was measured repeatedly
	The statistical test(s) used AND whether they are one- or two-sided Only common tests should be described solely by name; describe more complex techniques in the Methods section.
$\boxtimes$	A description of all covariates tested
$\boxtimes$	A description of any assumptions or corrections, such as tests of normality and adjustment for multiple comparisons
	A full description of the statistical parameters including central tendency (e.g. means) or other basic estimates (e.g. regression coefficient) AND variation (e.g. standard deviation) or associated estimates of uncertainty (e.g. confidence intervals)
	For null hypothesis testing, the test statistic (e.g. <i>F</i> , <i>t</i> , <i>r</i> ) with confidence intervals, effect sizes, degrees of freedom and <i>P</i> value noted <i>Give P values as exact values whenever suitable.</i>
$\times$	For Bayesian analysis, information on the choice of priors and Markov chain Monte Carlo settings
$\times$	For hierarchical and complex designs, identification of the appropriate level for tests and full reporting of outcomes
$\boxtimes$	Estimates of effect sizes (e.g. Cohen's <i>d</i> , Pearson's <i>r</i> ), indicating how they were calculated

#### Our web collection on <u>statistics for biologists</u> contains articles on many of the points above.

#### Software and code

Policy information about  $\underline{availability\ of\ computer\ code}$ 

Data collection

Live-cell images were taken by a Nikon Eclipse Ni-E upright microscope. The mcm5s2U tRNA modification was measured by LC-MS using an Agilent 6460 Triple Quadrupole mass analyzer running in MRM mode. Quantitative gene expression data was measured by a QuantStudioTM 3 Real-Time qPCR system (ThermoFischer Scientific, USA). Plate images were taken by a Canon PowerShot ELPH 360 HS with 12x optical zoom. Images of M. oryzae infected whole leaves were imaged by scanning using the EPSON Perfection V550 Photo.

#### Data analysis

Values represent the mean +/- SD of three independent biological replicates. Fluorescent protein distribution rates were analyzed using Microsoft Excel 2016. For comparing the mean values of the colony diameters, appressorium formation rates, penetration rates, and cell-to-cell movement rates, the one-way ANOVA function in PASW Statistics 18.0 (PASW Statistics Inc.) with the Tukey HSD multiple comparison test was used. For comparing the mean values of sporulation rates, the Welch ANOVA with Games-Howell post hoc test was employed. For comparing the mean values of lesion areas, statistical analysis was performed with two-tailed unpaired t-test or one-way ANOVA with Tukey's multiple comparisons test. For comparing target gene expression levels between different strains, the quantified transcript abundance was calculated as the fold change as described in the figure legends and statistical analysis was carried out using one-way ANOVA with the Student–Newman–Keuls test or the Tukey HSD multiple comparison tests in PASW Statistics. The R package agricolae was utilized to acquire precise P values for the Student-Newman-Keuls test, with modifications made to the source code of the SNK test function.

Live-cell images were processed by the software NIS-Elements (version 5.20.02). The mcm5s2U34 tRNA modification LC-MS data was analyzed using Agilent Qualitative Analysis software (B.07.00). The complete CDS database of Magnaporthe oryzae was obtained from the JGI Genome portal (https://genome.jgi.doe.gov/portal/pages/dynamicOrganismDownload.jsf?organism=Magor1, Project name: Pyricularia oryzae 70-15 v3.0). The codon usage pattern was analyzed using the CUSP program of EMBOSS (The European Molecular Biology Open Software Suite, Cambridge, UK; http://bioinfo.pbi.nrc.ca:8090/EMBOSS/) in R utilizing the high performance computing resources in Holland Computing Center at the University of Nebraska-Lincoln. qPCR data was analyzed using the QuantStudioTM Design & Analysis software package (Version 1.5.2).

For manuscripts utilizing custom algorithms or software that are central to the research but not yet described in published literature, software must be made available to editors and reviewers. We strongly encourage code deposition in a community repository (e.g. GitHub). See the Nature Portfolio guidelines for submitting code & software for further information.

#### Data

Policy information about availability of data

All manuscripts must include a data availability statement. This statement should provide the following information, where applicable:

- Accession codes, unique identifiers, or web links for publicly available datasets
- A description of any restrictions on data availability
- For clinical datasets or third party data, please ensure that the statement adheres to our policy

The M. oryzae UBA4 and URM1 gene sequences are available at NCBI (https://www.ncbi.nlm.nih.gov) under the accession numbers MGG\_05569 and MGG\_03978, respectively. Other gene sequences used in the course of this study can be found at NCBI under the following accession numbers: MGG\_13863 for PWL2, MGG\_10914 for BAS4, MGG\_15370 for AVR-Pita, MGG\_10097 for SLP1, FJ807764 for BAS1, MGG\_18041 for AvrPiz-t, MGG\_10020 for BAS107, MGG\_05785 for BAS113, JN035619.1 for AVR-Pik, AB434708 for Avr-Pia, AF463528.1 for AVR1-CO39, and AAK31287.1 for TOXB. Numerical and statistical source data that underlie the graphs in figures and extended data are provided with the paper. Strains generated during the course of this study are available from the corresponding author upon request and with an appropriate APHIS permit.

# Field-specific reporting

Please select the one below	v that is the best fit for your research.	If you are not sure, read the appropriate sections before making your selection. $ \\$
∠ Life sciences	Behavioural & social sciences	Ecological, evolutionary & environmental sciences

For a reference copy of the document with all sections, see <u>nature.com/documents/nr-reporting-summary-flat.pdf</u>

# Life sciences study design

All studies must disclose on these points even when the disclosure is negative.

Sample size

Sample size was chosen according to long-term experience in biological and biochemical experimentation, for example following Marroquin-Guzman et al. 2017, Nature Microbiology, and Li et al. 2020, New Phytologist. Pathogenicity-related assays were conducted according to published protocols. For inoculation assays, each independent experiment contains at least 3 randomly selected rice leaves. For analysis of the distribution of fluorescent proteins in growing fungal invasive hyphae, at least 50 invasive hyphae expressing fluorescent proteins were observed per replicate, n=3 biological replications.

Data exclusions

No data were excluded from analysis.

Replication

All experiments were performed in triplicate or with three biological replicates. All attempts at replicating the results were successful.

Randomization

Fungal strains were grown on complete media and randomly allocated for each experimental test.

Rice seedlings were grown under the same conditions and randomly allocated for the inoculation assays.

The distribution of fluorescent proteins in fungal invasive hyphae were observed in randomly selected infected rice cells.

Biological samples used in LC/MS analyses were selected by random sampling.

Blinding

Investigators were not blinded to group allocation during the experiments, but data collection and assessment were repeated by multiple independent experiments to ensure the analysis is as objective as possible.

# Reporting for specific materials, systems and methods

Harnie	5 5
hornone	0 7+0
_ _ _	5
Silin	2
sullillaly	3
	٦

	C	
c		
č	₹	
E		
	J	
C		
N		

We require information from authors about some types of materials, experimental systems and methods used in many studies. Here, indicate whether each material, system or method listed is relevant to your study. If you are not sure if a list item applies to your research, read the appropriate section before selecting a response.

Materials & experimental systems			Methods		
n/a	Involved in the study	n/a In	nvolved in the study		
X	Antibodies	$\boxtimes \Box$	ChIP-seq		
X	Eukaryotic cell lines	$\boxtimes   \Box$	Flow cytometry		
X	Palaeontology and archaeology	$\boxtimes   $	MRI-based neuroimaging		
$\times$	Animals and other organisms	·			
$\boxtimes$	Human research participants				
$\boxtimes$	Clinical data				
X	Dual use research of concern				